SPE-171193-MS

Measurement of Oil-Water Ratio and Formation Porosity Using Dielectric Spectroscopy in Borehole Environments

Timofey Eltsov, IPGG SB RAS; Vitaly Dorovsky, Baker Hughes Inc; Nikita Golikov, IPGG SB RAS; Leonty Tabarovksy, Baker Hughes Inc; Michael Epov, IPGG SB RAS

Copyright 2014, Society of Petroleum Engineers

This paper was prepared for presentation at the SPE Russian Oil and Gas Exploration and Production Technical Conference and Exhibition held in Moscow, Russia, 14–16 October 2014.

This paper was selected for presentation by an SPE program committee following review of information contained in an abstract submitted by the author(s). Contents of the paper have not been reviewed by the Society of Petroleum Engineers and are subject to correction by the author(s). The material does not necessarily reflect any position of the Society of Petroleum Engineers, its officers, or members. Electronic reproduction, distribution, or storage of any part of this paper without the written consent of the Society of Petroleum Engineers is prohibited. Permission to reproduce in print is restricted to an abstract of not more than 300 words; illustrations may not be copied. The abstract must contain conspicuous acknowledgment of SPE copyright.

Abstract

Finding water-oil rations in a saturated porous reservoir by means of EM logging is established on the possibility of imaging the dielectric spectra by the borehole inductive probe, identification of the components of the reservoir from these dielectric spectra, and determination of the water-oil ratio and porosity from the relaxation parameters. To find the water-oil ratio and porosity in the reservoir using dielectric spectroscopy, the mixing formula is often used. This formula expresses the complex dielectric permittivity via complex dielectric permittivities of the subsystems. Such a formula works in the MHz frequency range of the electromagnetic field. However, there are many problems associated with applying the mixing formulae. First, relaxation parameters of the Maxwell-Wagner polarization for the water-saturated porous media often fall outside of the domain where the Maxwell-Wagner polarization exists in reality and, as a result, the mixing formula is deemed inapplicable. Second, the number of relaxation parameters of the water-saturated porous medium (e.g. in the case when the formation is saturated with both water and oil) is typically lower than the number of dielectric degrees of freedom for the subsystems. Therefore, alternative methods are necessary to calculate bulk fractions of the subsystems present and formation porosity.

The lab study of dielectric spectra of sandstones and dolomites saturated with a water-oil mix demonstrates that elements of a qualitative difference between a water-saturated reservoirs can be introduced to that saturated with a water-oil mix using the acoustic frequency range of the electromagnetic field. This difference is from the huge values of dielectric polarization unrelated to the Maxwell-Wagner polarization. This paper shows that Havriliak-Negami dielectric spectra enable the introduction of a natural measure of water saturation in the samples saturated with a water-oil mix find the water-oil ratio. As a result, the universal dependence for finding porosity of the samples saturated with a water-oil mix is used. Knowledge ofa priori information regarding the material content of the reservoir is not necessary. The water-oil ratio and porosity depend exclusively on the Havriliak-Negami polarization parameters, which can be found univalently from the characteristic values of the parameters of the measured dielectric spectra.

Introduction

Finding the water-oil ratio in a saturated porous reservoir via borehole electromagnetic logging involves a wide range of dielectric spectroscopy issues. The solution to this problem depends, primarily, on the possibility of imaging the dielectric spectra using a borehole inductive EM probe (e.g. see [Hizem et al., 2008]), identification of the components of the saturated porous reservoir using the dielectric spectra (e.g. see [Revizsky, 2002]) and the possibility of finding the water-oil ratio from the fundamental relaxation characteristics of dielectric spectra [Hizem et al., 2008], [Seleznev et al., 2004]). The conceptual apparatus and methods of electric logging using the idea of electric conductivity of the medium with respect to direct current do not seem to suffice here. Furthermore, the frequency domain of the electromagnetic field defining the "zone of interest" in classic electric logging may be found only by studying the dielectric spectra, because the low-frequency Maxwell-Wagner asymptotics for high-resistivity media enable the identification of conductivity with respect to direct current from the dielectric spectra. On the other hand, it is conductivity with respect to direct current of the subsystems forming the porous that determines the relaxation parameters for Maxwell-Wagner polarization (e.g. see [Dukhin, Shilov, 1972]).

To find the porosity and water-oil ratio in the reservoir using dielectric spectroscopy, a mixing formula expressing the complex value of dielectric permittivity via complex values of dielectric permittivities of subsystems is often used. Typically, this comprises knowing whether the experiment agrees with the mixing formula [Seleznev et al., 2004]. By performing measurements of the dielectric spectrum in the frequency range of the electromagnetic field where Maxwell-Wagner polarization is definitely true, the relaxation parameters of the composite medium can be expressed via conductivities and dielectric permittivities of subsystems [Dukhin, Shilov, 1972]. In the borehole method, the relaxation parameters are found via measuring the dielectric spectrum by the electromagnetic inductive tool. When using the mixing formula, the conductivities and dielectric permittivities of subsystems are dicovered, as well as their bulk fractions, but serious problems can arise. First, the relaxation parameters of Maxwell-Wagner polarization for the porous water-saturated systems are often outside the domain where this polarization works and, thus, outside of the applicability domain of the mixing formula. Secondly, the number of relaxation parameters of the porous saturated medium (when the formation is saturated with both water and oil) is typically lower than the number of dielectric degrees of freedom for the subsystem. Therefore, alternative methods are necessary to find the bulk fractions of the subsystems involved and the formation porosity. The present article considers the possibility of measuring the porosity of the formation saturated with a water-oil mixture and finding the water-oil ratio from the spectrum of dielectric permittivity without including mixing formulae.

Acoustic Range of Electromagnetic Field

Identification of the water-and-oil-saturated porous medium using the dielectric spectra in the MHz range of the electromagnetic field (Maxwell-Wagner polarization domain) can be problematic. Fig. 1 and 2 show two typical spectra of dielectric permittivity in the MHz range for oil-saturated sandstone (Fig. 1) and water-saturated sandstone (Fig. 2) [Revizskij, Dyblenko, 2002].

Qualitatively, the frequency spectra behavior is identical: both curves have the Debye and Cole-Davidson polarization. The quantitative difference lies in the low-amplitude domains of the real and imaginary parts of dielectric polarization, which is compensated by formation porosity. It is difficult to identify the medium using only the dielectric spectra of oil and water. In the domain of MHz frequency and low dielectric permittivity, the colloid structure of the fluid overloads the spectra with data and complicates the identification of water, especially in the domains where its bulk fraction is small. The main reason why it is beneficial to measure and use the dielectric spectra in the MHz domain of the electromagnetic field frequencies is the availability of mixing formulae. The Bruggeman formula [Sen 1985], [Bruggeman 1935], [Hanai 1961] is the most often used (e.g. see [Seleznev et al., 2004]) because

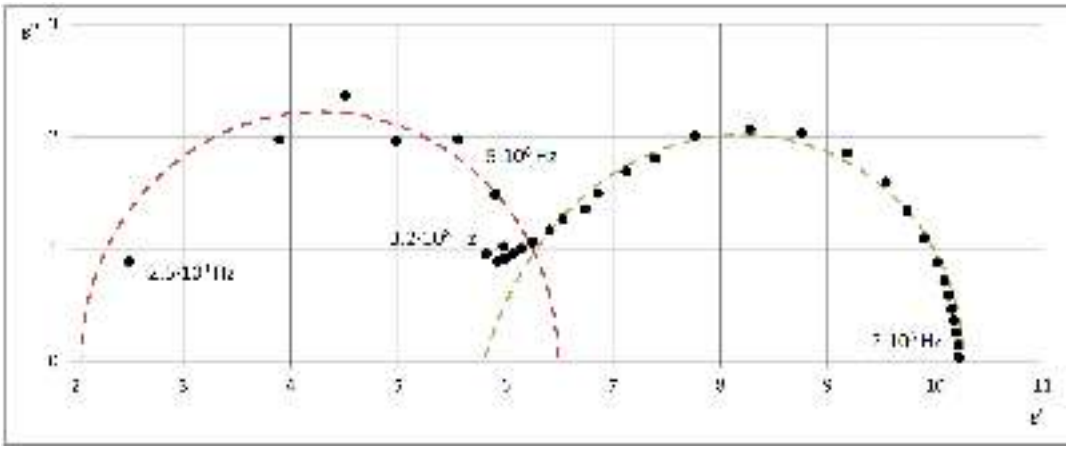

Figure 1—Dielectric spectrum for oil-saturated sandstone [Revizskij, Dyblenko, 2002].

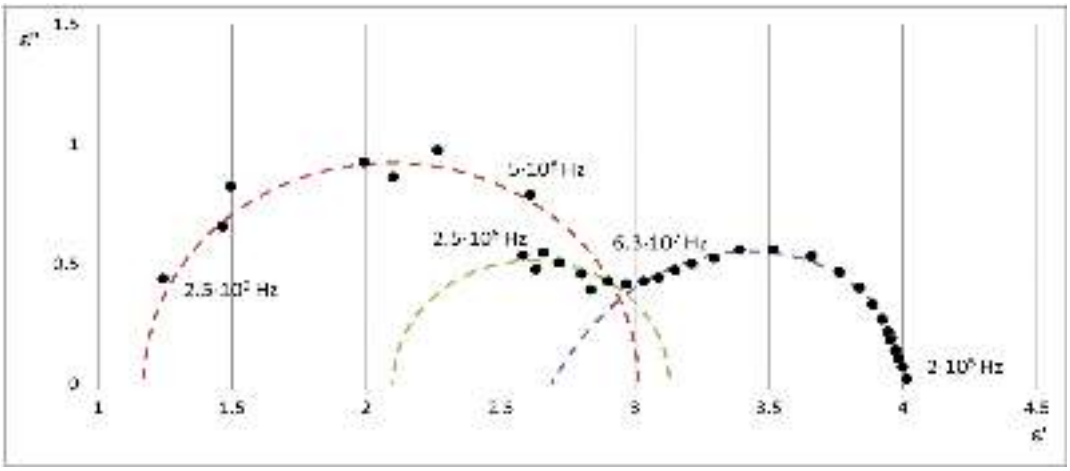

Figure 2—Dielectric spectrum for water-saturated sandstone [Revizskij, Dyblenko, 2002].

it accurately describes dielectric permittivity of the composite "carbonates plus brine." The basis of the physical mechanism behind the mixing formula is the vagrant currents flowing through the volume of the subsystems of which the dielectric composite is made, and which cause the Maxwell-Wagner polarization. However, it is possible to qualitatively identify water-saturated porous media within borehole conditions by widening the frequency range of the electromagnetic field to the kHz domain. [Levitskaya, Nosova, 1984] and [Levitskaya, Palveleva, 1990] demonstrate that the polarization dielectric spectrum of water-saturated dolomites and sandstones may be described by the symmetrical Cole-Cole curve in the 10 kHz-60 MHz frequency domain (Fig. 6, the curve with circles). In the kHz frequency domain (acoustic frequency range), the real part of dielectric permittivity may reach 400 and up at a water saturation of 6.6%. Such high values of dielectric permittivity in porous water-saturated media at low water concentration may not be achieved by means of the mechanism behind the Maxwell-Wagner polarization. The symmetrical dielectric spectrum of water-saturated rocks and high values of dielectric permittivity in the kHz frequency domain of the spectrum may signal the presence of water in the porous medium and thus, serve as the basis of the method for finding water saturation in the borehole methods of dielectric spectroscopy. On the other hand, no Maxwell-Wagner polarization mechanism means the mixing formula cannot exist. This is obvious if the mechanism of dielectric polarization derives from the counter-ion motion in the double electric layer [Dukhin, Shilov, 1972]. The double electric layer separates water and rock in the porous space. The vagrant currents in the rock are small and, compared to the huge polarization capacity of the double electric layer, are bypassed and are not observed in the dielectric spectra. Therefore,

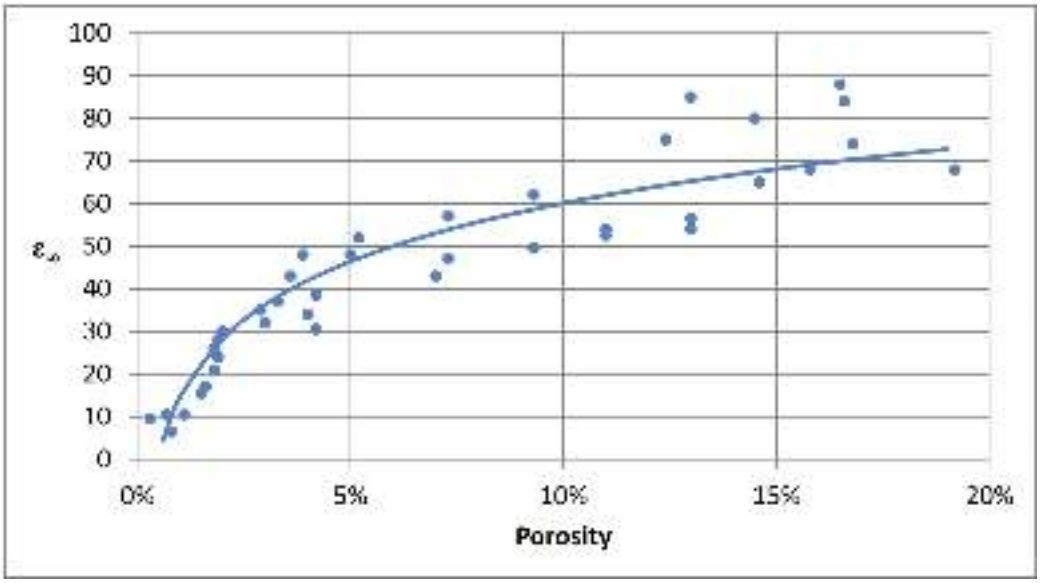

Figure 3—Dependence of the high-frequency limit of the real part of dielectric permittivity upon porosity [Levitskaya, Nosova, 1984].

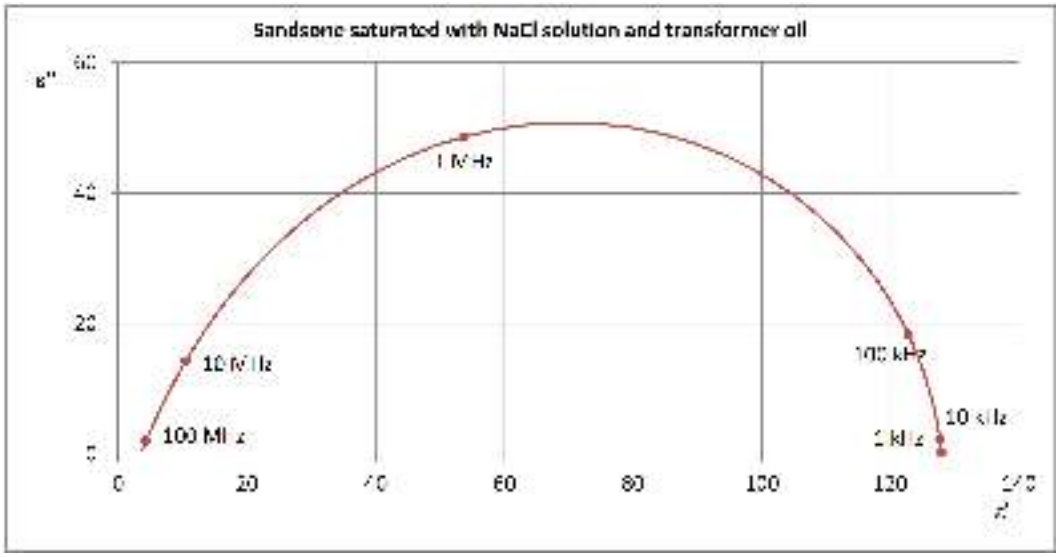

Figure 4—The Havriliak-Negami dielectric spectrum: dielectric permittivity of sandstone (porosity 14.1%) saturated with NaCl solution (concentration 15 g/l), and that saturated with transformer oil (7.61% of the pore volume). [Levitskaya, Palveleva; 1990].

we are unable to see dielectric permittivity of the rock when water is present and, thus, no corresponding mixing formula is obtained.

Levitskaya and Nosova [Levitskaya, Nosova, 1984] established that the asymptotic value of the real part of dielectric permittivity in the high frequency domain does not depend much on formation lithology. It is possible to identify rock types (clastic, chemogenic, organogenic, etc.), where this dependence is extremely weak. Furthermore, the asymptotic (high-frequency) value of the real part of dielectric permittivity in the high frequency domain does not depend on the salinity of the brine saturating the porous medium [Levitskaya, Nosova, 1986]. It is easier to understand if the Maxwell-Wagner mixing formula is taken into account, which is always true in the high frequency domain of the spectrum (where the high-frequency, asymptotic value of the real part of dielectric permittivity does not depend on conductivities of the subsystems with respect to the direct current and in accordance with the mixing formula). Fig. 3 shows the dependence on water saturation (porosity) as a characteristic function of what?

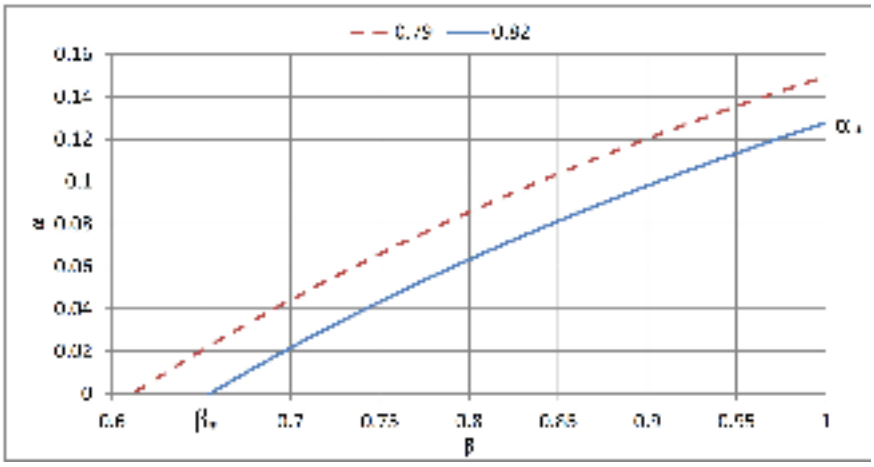

Figure 5—Dependence (3) for two values of the parameter $2\varepsilon'_{max}/\Delta\varepsilon$.

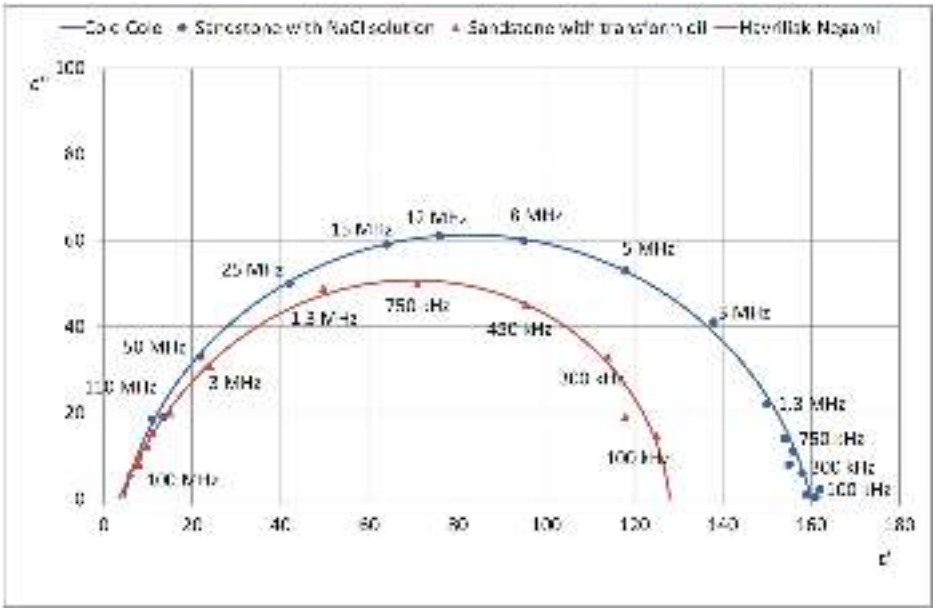

Figure 6—Dispersive polarization curve for sandstone saturated with brine $(\beta = 1, \Delta\varepsilon = 151.5, \varepsilon'_{max} = 61.2)$ and for sandstone saturated with brine and transformer oil $(\beta = 0.718, \Delta\varepsilon = 124.3, \varepsilon'_{max} = 50.8)$, [Levitskaya, Palveleva, 1990].

The character of dependence significantly differs from the corresponding dependence of the Maxwell-Wagner polarization [Dukhin, Shilov, 1972]. It is important to notice the rapid growth of the asymptotic value of dielectric permittivity in the domain of low water concentrations, whereas the Maxwell-Wagner polarization is characterized by the rapid growth of dielectric permittivity only in the domain of high water concentrations. The curve in Fig. 3 enables the obtaining of water saturation and thus, porosity of the water-saturated formation within the framework of the absolute measurement scale if the value is known. Knowing the measured enables the percentage K of water present in pores to be obtained from the curve. Before that, the water saturation can be confirmed of the formation from the Cole-Cole polarization curve.

Using the results of experimental research performed by Levitskaya and Palveleva [Levitskaya, Palveleva, 1990], the signs of oil and water in the formation pores can be identified. The dielectric spectrum of the formation saturated with the water-oil mixture is characterized by the Havriliak-Negami polarization curve [Chelidze, 1977]. The Havriliak-Negami curve is asymmetric in the domains of high and low frequencies of the magnetic field.

Table 1—Sandstone specimens of the West Siberian oil deposit, h – specimen height, K_p – porosity.

№	h, mm	K_p, %	Notes
70	30	11.96	Inclusions of ferrous material
79	10	13.54	Sandstone
79	30	13.54	Sandstone
83	30	11.34	Sandstone
87	30	17.56	Sandstone
94	25	15.8	Carbonate
96	30	15.75	Grainy sandstone
103	30	19.38	Sandstone
104	25	18.13	Sandstone
108	25	13.74	Sandstone
109	30	12.73	Inclusions of clay
201	30	15.5	Carbonate, 50% oil
202	30	20.53	Sandstone, 60% oil

When measuring the spectrum of dielectric permittivity by an inductive borehole tool, the asymmetry of the polarization curve and fairly high values of dielectric permittivity must be attributed to the presence of oil in addition to water. However, the slight asymmetry may be also caused by organic material present in the system [Levitskaya, Palveleva, 1984].

Finding formation porosity

Finding porosity in the presence of random oil content in the pores may be problematic if using the method described above. The Havriliak-Negami polarization curve:

$$\varepsilon = \varepsilon' + i\varepsilon'' = \varepsilon_\infty + \frac{\varepsilon_0 - \varepsilon_\infty}{[1 + (i\omega\tau)^{1-\alpha}]^\beta} \tag{1}$$

yields a formula that link the polarization degrees α, β to the polarization parameters of the Cole-Cole curve [Derevyanko, Kurilenko, 1971]:

$$\frac{2\varepsilon''_{max}}{\Delta\varepsilon} = \sin\left(\frac{1-\alpha}{4}\pi\right) \cdot \chi(\beta), \qquad \chi(\beta) = \left[\sin\frac{\beta\alpha}{2(1+\beta)}\right]^{1-\beta} \tag{2}$$

In formulae (1) and (2), the following notations are used: ε is the complex value of dielectric permittivity, ε_∞ is the high-frequency limit of the real part of dielectric permittivity, ε_0 is the value of dielectric permittivity at $\omega = 0$ and τ is the characteristic relaxation time.

The parameter β varies, generally, within the interval [0, 1], and the value $\beta = 1$ corresponds to scenarios when there is no oil in the pore space. The parameter α also varies within the interval [0, 1], but the value $\alpha = 0$ corresponds to scenarios where there is no water in the pore space of the formation.

The latter formula can be solved with respect to the polarization parameter α (Fig. 5):

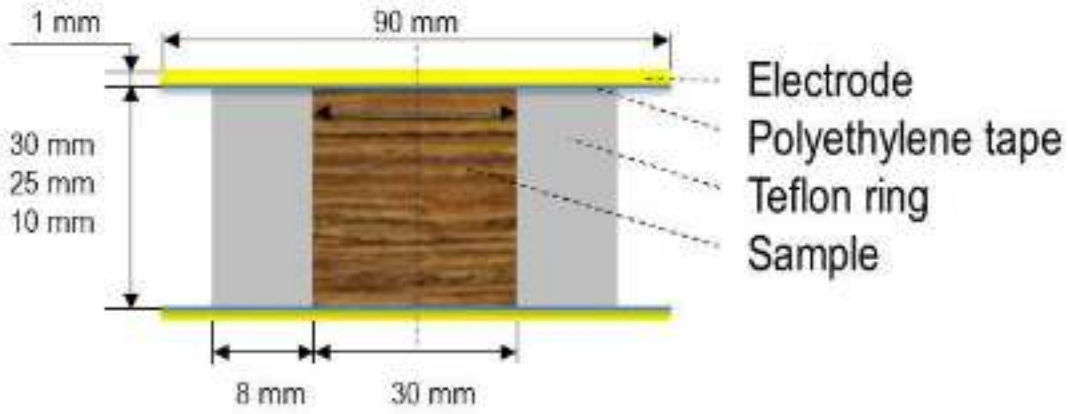

Figure 7—The capacitor cell: a flat capacitor with cylindrical plates, polyethylene insulator pad, Teflon liner and a rock specimen.

Table 2—The results of selecting the equivalent circuit parameters corresponding to the specimens saturated with distilled water. Porosity K_p is provided for the sake of comparison with the parameter α, which is equivalent to porosity at 100% water saturation.

N o.	h. mm	C_∞ / C_0	C_0 / C_∞	C_∞	τ, μs	α·100 %	K_p, %
7 0	39	61.89	2.09		0.1 4	2.3%	11.96
7 9	6	169.16	7.47	-	0.1 81	2.34 %	13.94
7 9	8	43.54	10.5 8	8.87	0.7 52	2%	13.94
8 3	80	92.94	2.58	-	0.2 16	11.56 %	11.34
8 7	80	97.3	2.6	0.835	0.3 0	14.75 %	12.56
9 1	25	114.39	0.5	1.05	0.1 168	15.7%	15.8
9 e	30	75.8	1.58 4	-	0.1 23	5.9%	15.75
1 08	25	141.5	2.78 9	0.806	0.2 72	4.3%	13.76

$$\alpha = 1 - \frac{1}{\pi} \arctg \frac{2\varepsilon''_{max} / \Delta\varepsilon}{\chi(\beta)} \quad (3)$$

Fig. 6 shows two polarization curves for sandstone: one curve corresponds to a scenario when only brine is present in the formation pores, and the other curve, with a smaller maximal amplitude of the imaginary part of dielectric permittivity, corresponds to a scenario when transformer oil is present in addition to brine (54% - oil, 46% - water, formation porosity - 14.1%). For these two curves, the value is the same as the parameter $2\varepsilon''_{max} / \Delta\varepsilon \approx 0.8$, as it follows from the graph in Fig. 6 and from the data reported in [Levitskaya, Palveleva, 1990]. In other words, the parameter $2\varepsilon''_{max} / \Delta\varepsilon$ is a weak function of oil content: for the same porous medium saturated with different proportions of oil and water, the value $\nu = 2\varepsilon''_{max} / \Delta\varepsilon$, remains practically the same. The value $2\varepsilon''_{max} / \Delta\varepsilon$ is a characteristic of the porous space saturated with water. The parameter β may be interpreted as the parameter characterizing the presence of oil. In the presence of oil, each value β not equal in unity corresponds to the value α_v (β) found via (3). For each given value $2\varepsilon''_{max} / \Delta\varepsilon$, the parameter characterizing oil saturation β may only vary within the interval[β_*, 1] as shown in Fig. 5, where $\beta = 1$ corresponds to the scenario with no oil. The value $\beta = \beta_*$ corresponds to the scenario with no water in the formation pores. At the same time, the polarization

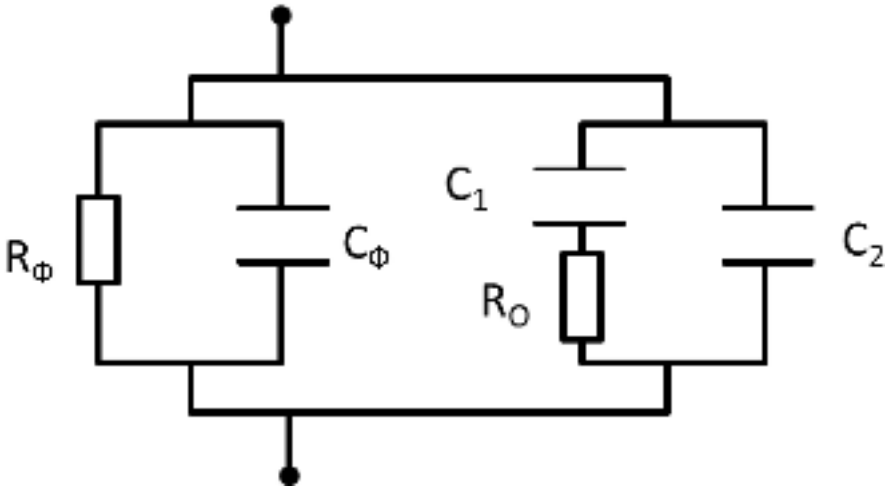

Figure 8—The simplified equivalent circuit of the capacitor with the specimen and Teflon liner. R is resistance and C is capacity. Indices: Φ denotes PTFE and O denotes the specimen

$$C_{\Phi} = C_0(\varepsilon_{\Phi} - \varepsilon_{\infty}), C_1 = C_0\varepsilon_{\infty}, \quad R_{\Phi} = \nu\left[1 - \left|1 - (i\omega\tau)^{1-\alpha}\right|\right] \div \omega C_0$$

parameter α varies within [0, α]. The values α_*, β_* at a given ratio $2\varepsilon''_{max} / \Delta\varepsilon$ arefound from the following equations:

$$\chi(\beta_*) = \nu, \tag{4}$$

$$\alpha_* = 1 - \frac{4}{\pi}\operatorname{arctg}\nu \tag{5}$$

There is a link between the values α_*, β_*:

$$\chi(\beta_*) = \operatorname{tg}\frac{1-\alpha_*}{4}\pi \tag{6}$$

At $\beta = 1$ there is no oil in the pores, and thus, α_* determines the limit water saturation or porosity. At $\nu = 0.8$, in accordance with the dielectric spectrum of the water-saturated sandstone sample and of that saturated with water and transformer oil [Levitskaya, Palveleva, 1990], the limit water saturation is 14 % as per formula (5). On the other hand, according to [Levitskaya, Palveleva, 1990], who directly measured the porosity of their samples, porosity was found to be 14.1%. This is in agreement with the measurement error bar. For dolomites, [Levitskaya, 1984] there is $2\varepsilon''_{max} / \Delta\varepsilon = 0.71$ and the limit saturation is approximately18% as per (5). The experiment yield is 16.9%, which means that porosity K in percent may be calculated using the formula:

$$K = \alpha_* \times 100\% \tag{7}$$

It becomes evident why α_* was introduced as the parameter of water saturation.

Thus, the method of measuring formation porosity in a borehole, under the conditions of the pore space being saturated with a water-oil mixture, can be reduced to the following procedure. Using the characteristics of the dielectric spectrum, we can calculate $\nu = \nu_0 = 2\varepsilon''_{max} / \Delta\varepsilon$. The degree of polarization $\Delta\varepsilon = \varepsilon_0 - \varepsilon_\infty$ must be known in addition to the maximum value of the imaginary part of dielectric permittivity ε''_{max} in the Havriliak-Negami polarization. Formula (3) determines the relationship of formation parameters with water and oil saturation (one chooses the curve of this functional family $\alpha_\nu(\beta)$, characterizing the formation under study at a given $\nu = \nu_0$). The limit value $\alpha_* = \alpha_{\nu 0}$ ($\beta = 1$) determines the state of the formation when there is only water in the pores. Porosity is found from formula (7).

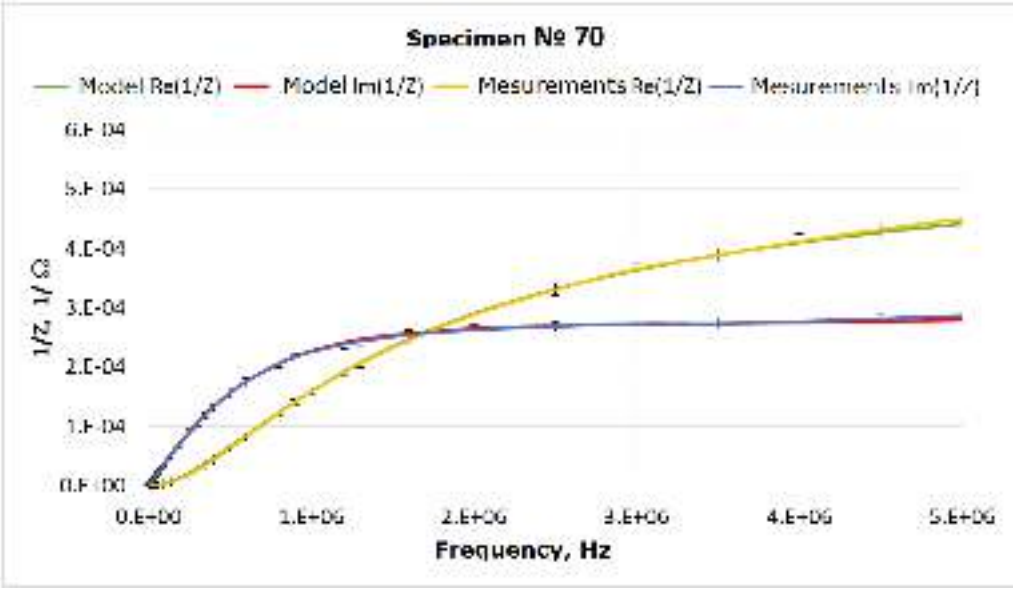

Figure 9—The results of selecting the equivalent circuit parameters (sandstone, specimen No. 70).

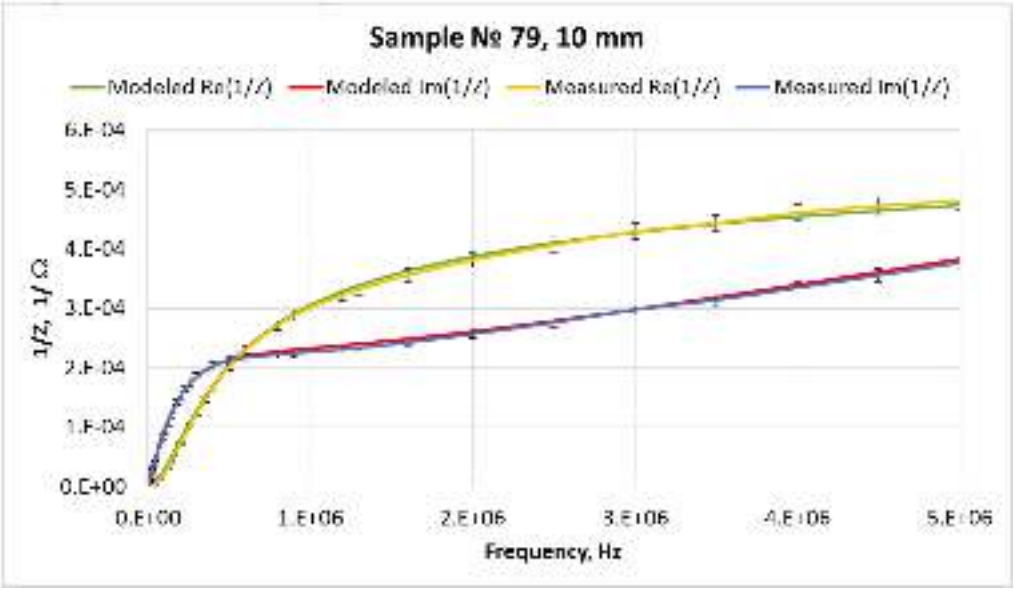

Figure 10—The results of selecting the equivalent circuit parameters (sandstone, specimen No. 79).

In the calculations of $\Gamma - \Sigma_{inv}^{E} / \Delta\varepsilon$ above, the values of the relaxation parameters are taken directly from the graph and contain small errors. In the publication by [Levitskaya, Palveleva, 1990], the relaxation/polarization parameters for sandstones are given, but, unfortunately, the polarization parameter α is not listed (only the polarization curve parameter β for Havriliak-Negami polarization is provided). For this reason, it appears impossible to use the numerous data listed in the tables. In reality, only four graphic representations of this material can be used, which confirm the proposed method of measuring porosity from dielectric spectra.

Thus, the procedure described above enables porosity to be found from the polarization curve. The problem is reduced to finding the spectrum with the inductive borehole tool. In spite of the need to know only three relaxation parameters of the dielectric spectrum, it is necessary to measure the entire spectrum (with a reasonable resolution with respect to frequency) within the borehole conditions, throughout the

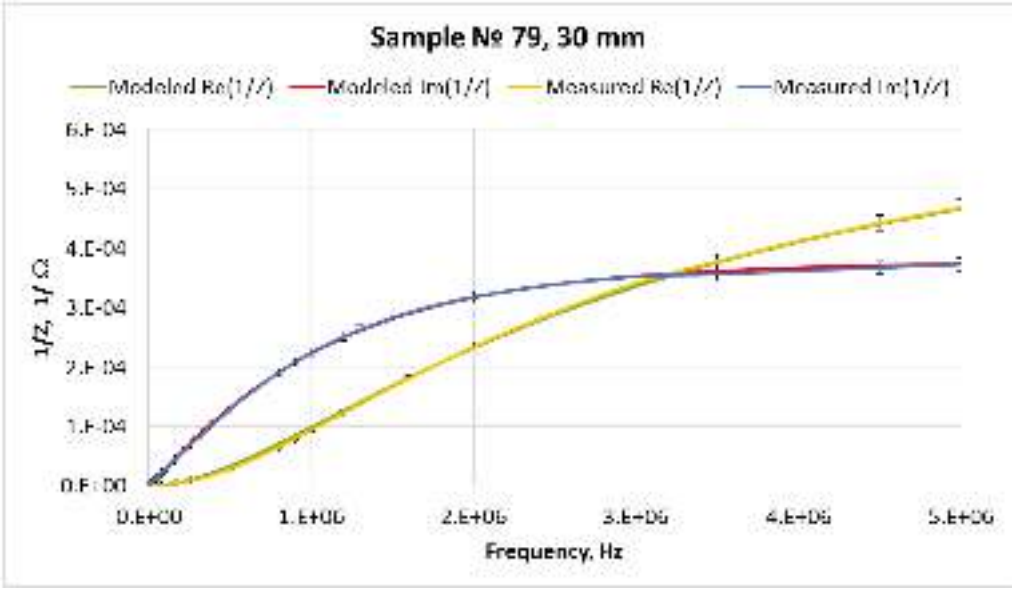

Figure 11—The results of selecting the equivalent circuit parameters (sandstone, specimen No. 79).

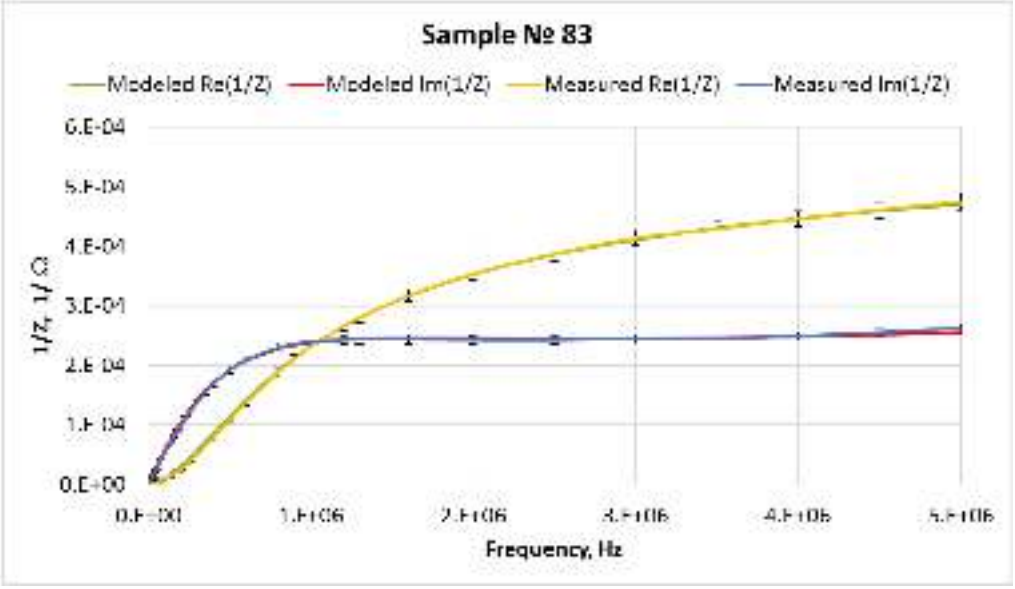

Figure 12—The results of selecting the equivalent circuit parameters (sandstone, specimen No. 83).

entire acoustic range of the electromagnetic field, because it is necessary to establish that it is the Havriliak-Negami polarization and that the system is saturated with a water-oil mixture. Additionally, the choice of frequencies of the electromagnetic field may be influenced by the depth of the measurements, the design of the electromagnetic probe or external criteria.

Oil saturation is determined by the parameter β, which corresponds to the value α as per formula (2). There is a natural comparison scale for water saturation of the medium under borehole conditions while the inductive tool is running down inside the borehole. The water fraction in the pore space in percent is found using the formula:

$$K_w = \frac{\alpha}{\alpha_z} 100\%,$$

The oil fraction in percent is found using the formula:

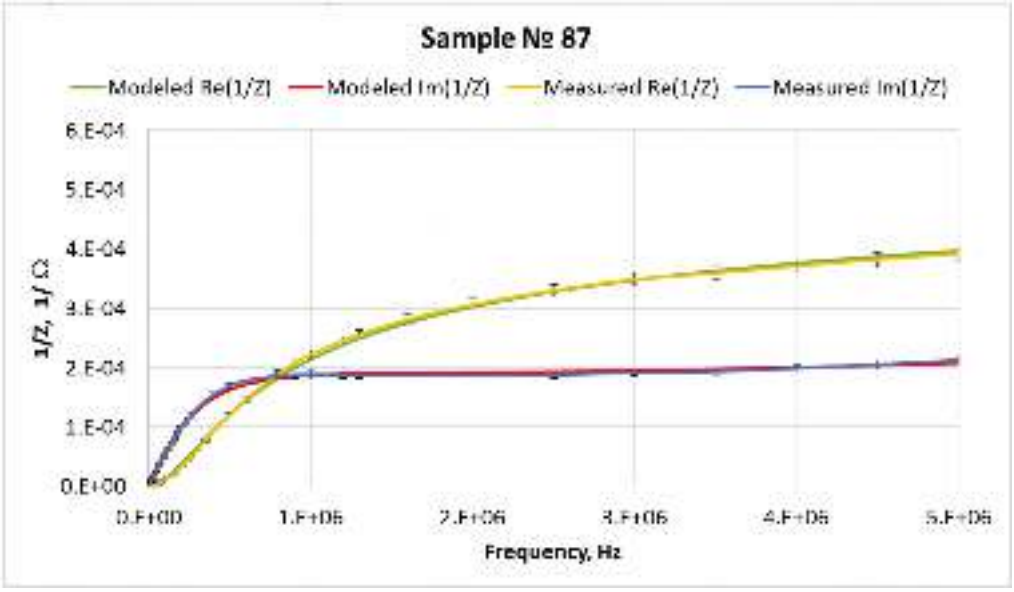

Figure 13—The results of selecting the equivalent circuit parameters (sandstone, specimen No. 87).

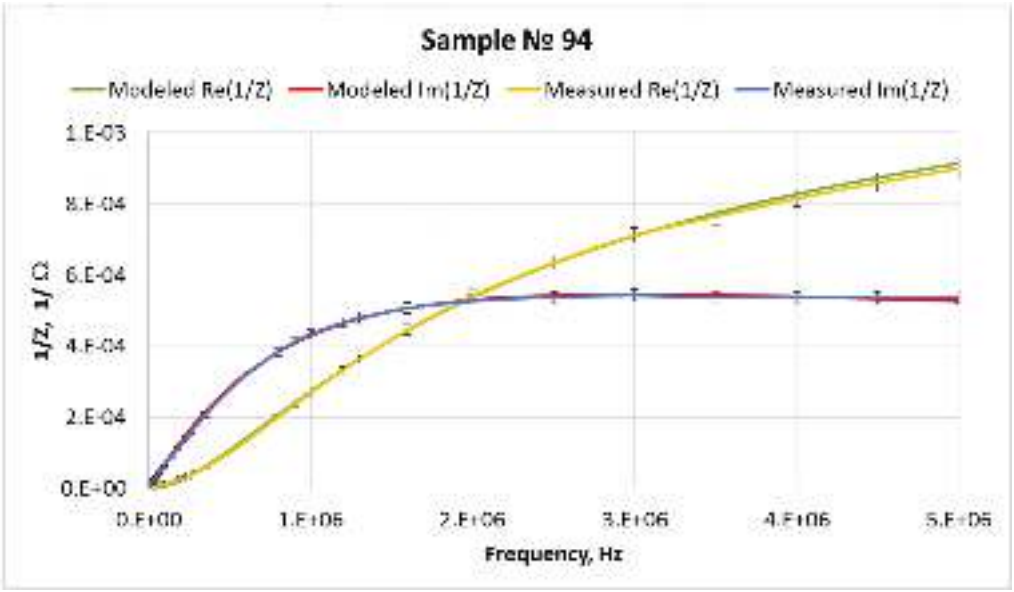

Figure 14—The results of selecting the equivalent circuit parameters (carbonate, specimen No. 94).

$$K_{oil} = \left[1 - \frac{\alpha(\beta)}{\alpha_*(\beta_*)}\right] 100\%.$$

The measurement scale is relative. To introduce an absolute measurement scale, the relative scale must be marked by performing lab measurements. At the same time, porosity measurements in accordance with formula (7) are performed using the absolute measurement scale.

Samples and laboratory studies

In addition to the experiments reported by Levitskaya and Pelveleva [Levitskaya, 1984; Levitskaya, Pelveleva, 1990], laboratory studies aimed at measuring the dielectric spectra of sandstones and carbon-

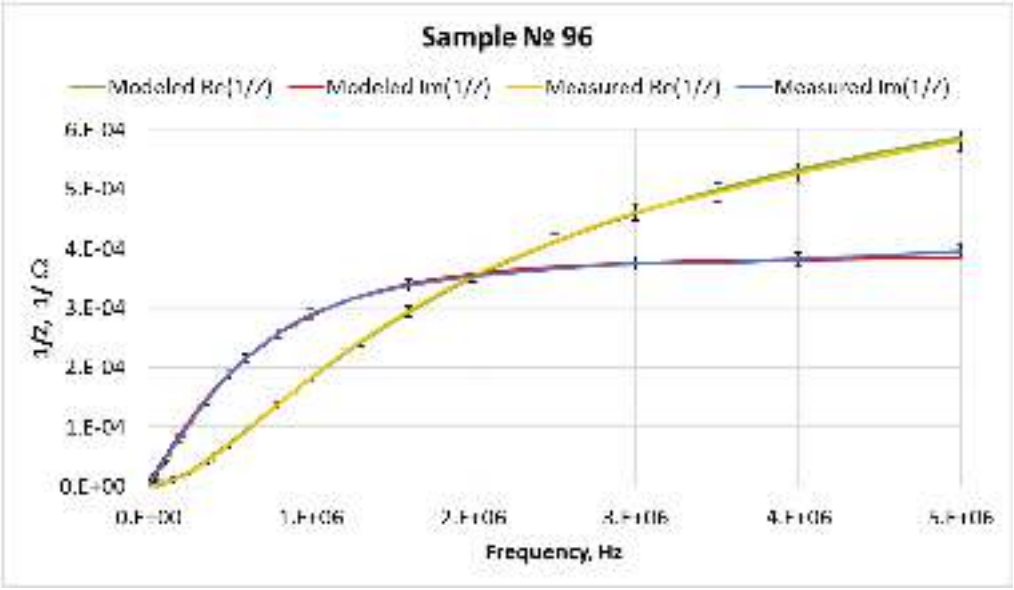

Figure 15—The results of selecting the equivalent circuit parameters (sandstone, specimen No. 96).

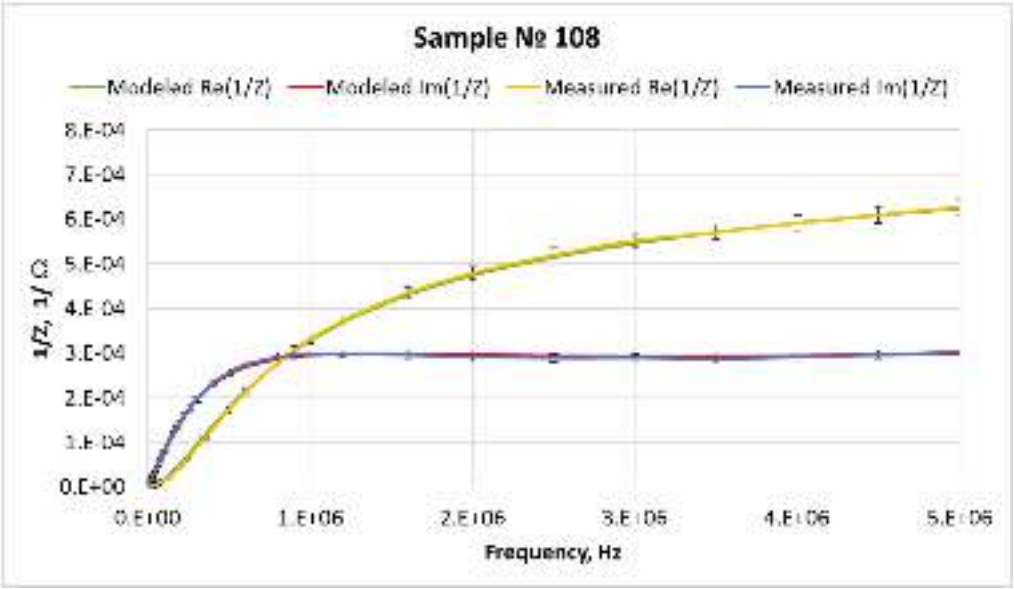

Figure 16—The results of selecting the equivalent circuit parameters (sandstone, specimen No. 108).

ates saturated with water or a water-oil mix were performed to verify the proposed method of measuring porosity and water-oil ratio. Sandstone and carbonate specimens of various lithology and petrophysical parameters were collected. These specimens represented typical reservoirs of the West Siberian oil deposit. These specimens were reduced to the size of a measuring capacitor cell and PTFE rings (cylinders, diameter: 30 mm, height: 30, 25, and 10 mm) and their edges were polished. The cores were washed and dried to remove residual moisture and the dry specimens were weighed. These specimens were saturated with distilled water during 72 hours within vacuum conditions. The saturated specimens and specimen in water were weighed. Specimens No. 201 and 202 were partially saturated with transformer oil. The oil content in pores was monitored by weighing, and after that, measurements in the capacitor cell were performed.

To measure dielectric permittivity, a capacitor cell was made of brass, polyethylene and Teflon.

Table 3—The results of selecting the equivalent circuit parameters and corresponding to the specimens saturated with transformer oil. $K_{o.m.}$ is oil content measured in the lab, $K_{o.c.}$ is oil content calculated theoretically and α^* corresponds to porosity (K_p).

	20			1	0.2		0.15	0.0	0	15.		1
	20	0	2.7	55	0.2	3	72	0.0	56	20.	0	8
2		0	3.1	63	65	4	77		65	53	0	11

Capacity measurements for the capacitor cell were performed within the 50 kHz to 6 MHz frequency range using the LCR GW Instek 78105G measurement tool and Rohde and Schwarz's ZVRE vector circuit analyzer.

A cylindrical specimen was placed into the ftoroplast ring and into the capacitor cell, where the impedance module and phase were measured using the LCR measurement tool. The transmission coefficient, S_{21}, was measured using the ZVRE vector analyzer. The polyethylene adhesive tape was attached onto the electrodes to eliminate the influence of natural polarization. Dielectric losses in polyethylene are almostzero, while the real part of dielectric polarization is 2.2 within the 50 kHz to 100 MHz frequency range; there is no dielectric dispersion within this frequency range.

To achieve a more even distribution of fluid in the pore space, larger specimens were used in the capacitor cell and the ratio of electrode diameter to the distance between the electrodes was equal to 3. In addition, the height of specimen No. 79 was made 10 mm and the ratio of electrode diameter to the distance between the electrodes was equal to 9 (which is close to the "flat capacitor" approximation). The measurement results for specimen No. 79, height: 10 mm and 30 mm, were compared (see Table 2).

The key feature of this capacitor design is the presence of the polyethylene film and PTFE ring. The polyethylene film eliminates natural polarization. The PTFE liner prevents deformation of capacitor plates after the capacitor is further compacted. Such a composite capacitor has interfaces with the specimen under study and conveys additional frequency dependence into the system's impedance, which must be separated from the frequency dependence of the complex dielectric permittivity of the specimen.

The measurement cell was compared with the simplest equivalent circuit shown in Fig.8.

The diagram of the semistationary circuit in Fig.8 shows two parallel impedances: the capacitor part with the Teflon liner and the capacitor part with the specimen under study. The impedance of the capacitor and specimen $Z_{0+\Phi}$ was measured first, then the specimen was taken out, and the impedance Z_Φ of the capacitor with no specimen was measured (only the Teflon liner was left in the capacitor). The experimentally obtained parameter $1/Z_{0+\Phi} - 1/Z_\Phi$ equals $i\omega C(\omega)$in the simplified semi-stationary circuit where $C(\omega)$ is the complex capacity of the capacitor with the specimen and $C'(\omega) - C_0\varepsilon'(\omega)$. $\varepsilon(\omega)$ is the complex dielectric permittivity of the specimen corresponding to the Havriliak-Negami polarization, equation (1).

Joining the theoretical frequency dependence $i\omega C(\omega)$ and measured $1/Z_{0+\Phi} - 1/Z_\Phi$ frequency dependence, the semistationary circuit parameters C_1, C_2, α, β, τ, can be obtained in addition to the polarization parameters α, β. Using the last two parameters, the porosity water-oil ratio of the specimen is found in accordance with the method described above. The simplified semi-stationary circuit does not take into account the polyethylene film present in the capacitor because only the 50 kHz to 6 MHz frequency range is used. Figs.9 to 18 demonstrate the results of selecting the equivalent circuit parameters for the specimens under study. Each graph shows combinations of the measured values of the real and imaginary parts of the complex frequency function $1/Z_{0+\Phi} - 1/Z_\Phi$ and corresponding theoretical curves computed

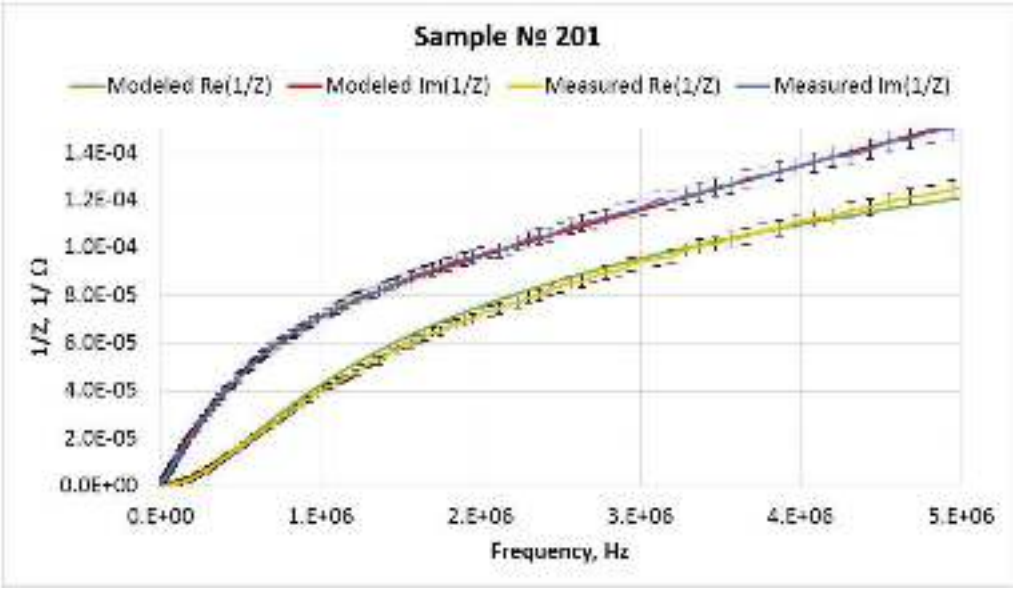

Figure 17—The results of selecting the equivalent circuit parameters (carbonate, specimen No. 201).

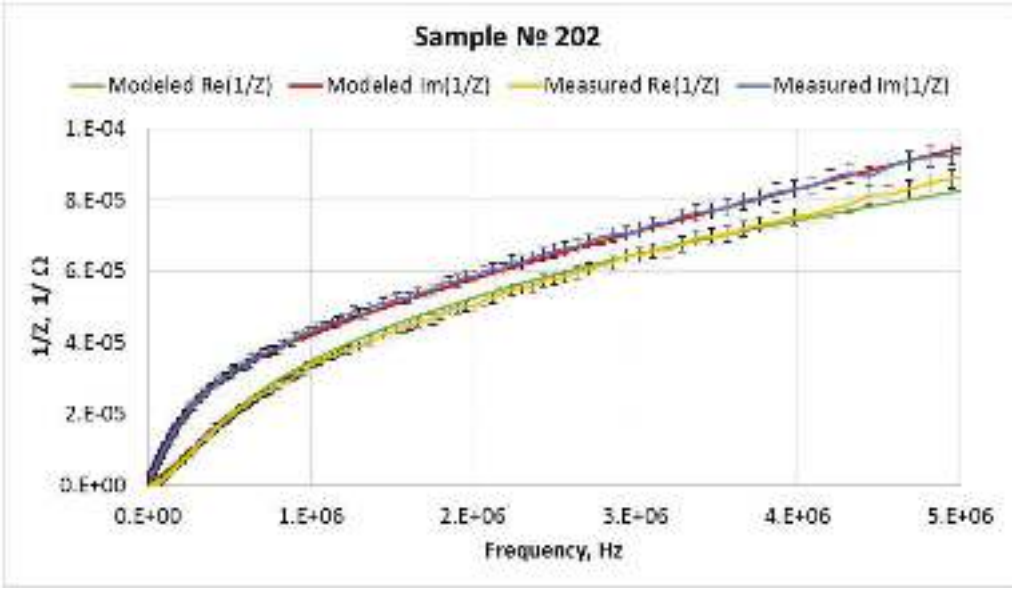

Figure 18—The results of selecting the equivalent circuit parameters (sandstone, specimen No. 202).

under assumption that polarization in the specimens is Havriliak-Negami. Selection of the parameters for the theoretical model (Havriliak-Negami) was performed using standard procedures of the mathematical Kernel software package (Wolfram, 2014). There was good agreement between the results of the theoretical curves corresponding to the Havriliak-Negami polarization and the laboratory data obtained within the 50 kHz to 6 MHz frequency range. The frequency-dependent curves coincide within the measurement error bar throughoutthe entire frequency range indicated. Parameters α, β were found exclusively within the frequency range indicated.

Table 2 lists the parameters selected for the equivalent circuit for the specimens saturated with distilled water (α corresponds to porosity). Theoretically found porosity agrees well with porosity found in the lab.

The specimens saturated with water and model oil (Fig.17 and 18) were investigated. Having α and β (Table 3) enables the calculation of parameter ν using formula (2). Parameter ν can enable the universal

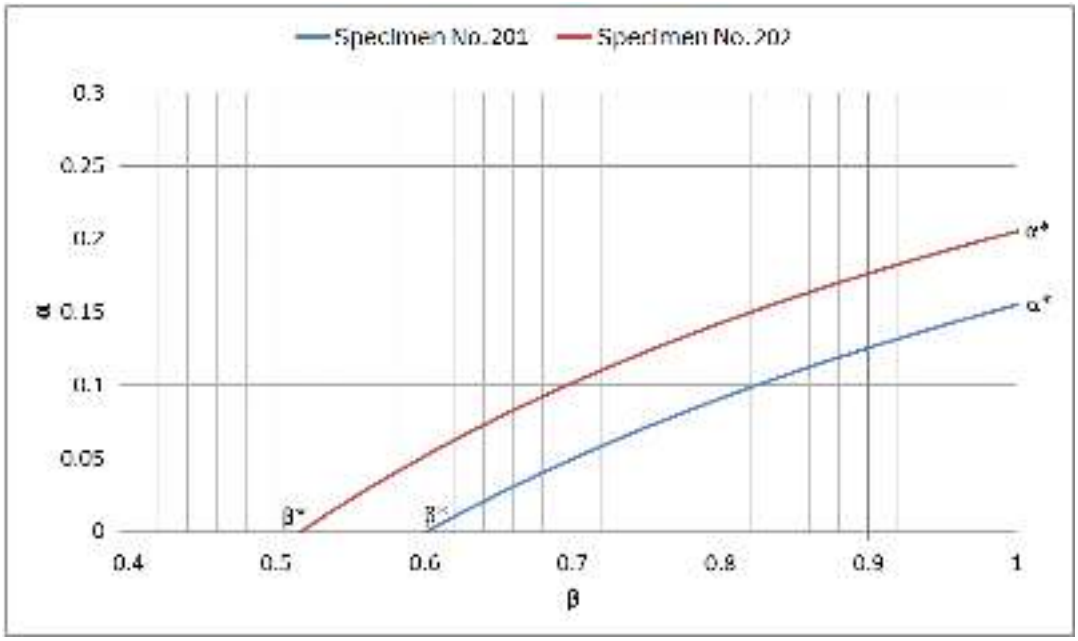

Figure 19—Dependence $\alpha_r(\beta)$ for specimens No. 201, No.202, saturated with water and oil.

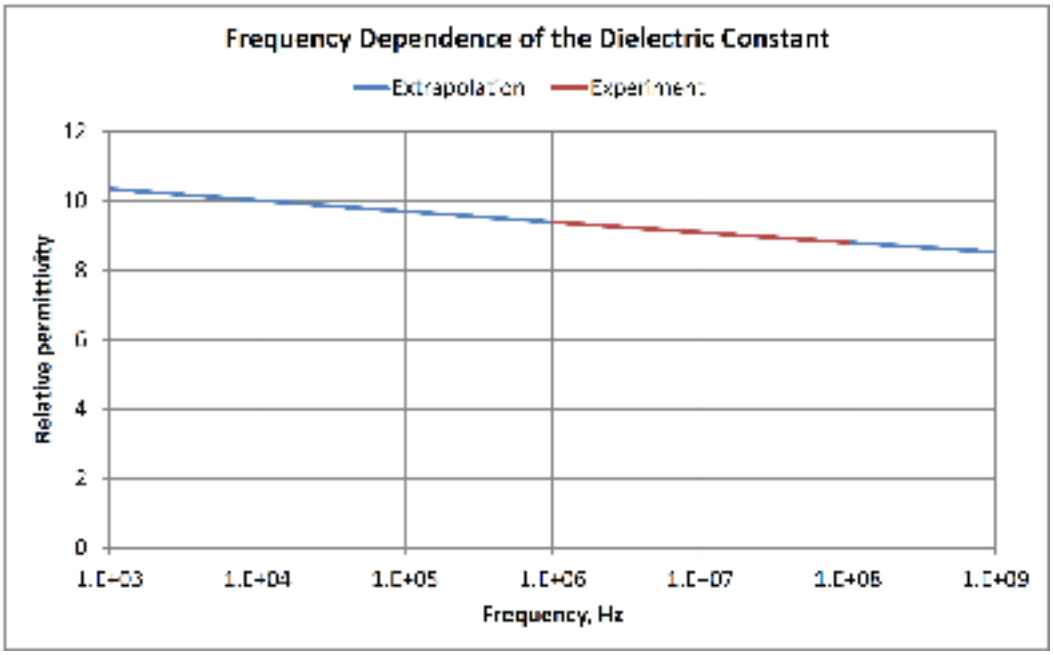

Figure 20—Frequency dependence of the real part of dielectric permittivity of oil-based mud. The solid line corresponds to the experimental data [Patil et al. 2010] and the dashed line corresponds to linear extrapolation of measurements into the low-frequency domain.

dependence to be found of α upon β specimens No. 201 and No. 202. For the fixed β, α is obtained. The curve $\alpha(\beta)$ at $\beta=1$ yields porosity α^*. Therefore, the water content (in percent) is obtained using formula (8): $100\% \cdot \alpha(\beta)/\alpha^*$.

The agreement between porosity measured in the lab and that calculated theoretically, as well as the agreement between the oil content measured in the lab and that calculated theoretically, indicates:

- The method proposed for finding water and oil content confirms that it is the Havriliak-Negami polarization (10) that takes place within this frequency range

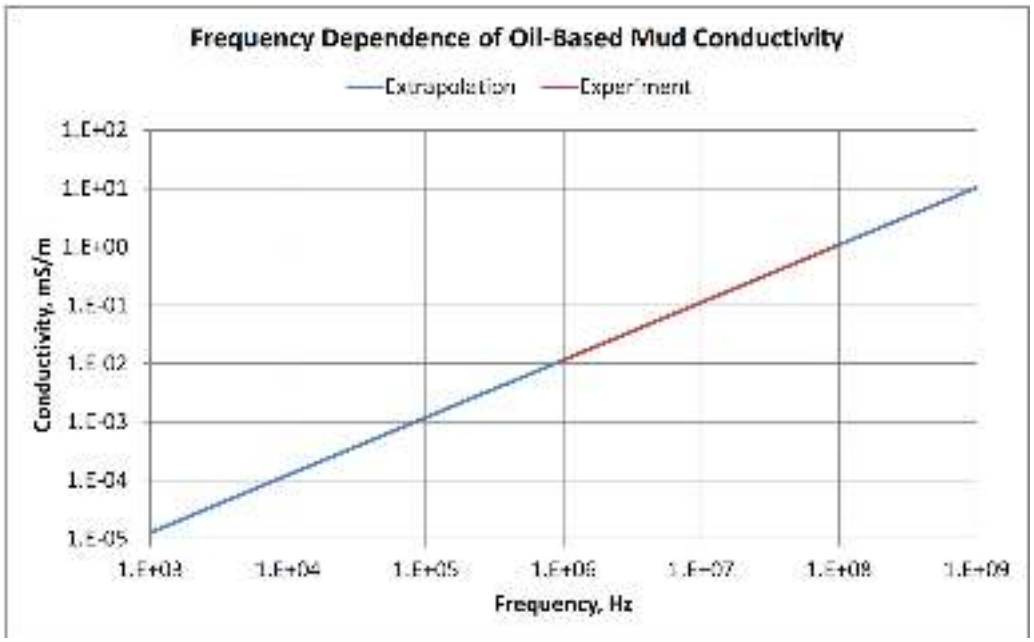

Figure 21—Frequency dependence of electric conductivity of oil-based mud. The solid line corresponds to the experimental data [Patil et al. 2010] and the dashed line corresponds to linear extrapolation of the results into the kHz domain of the electromagnetic field.

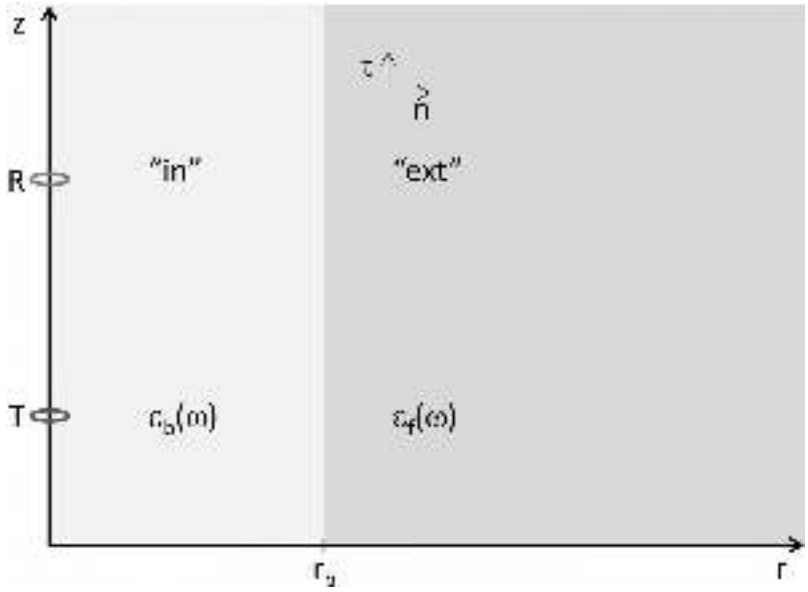

Figure 22—The computational model of the medium: "borehole plus formation." In this model, the borehole radius and the frequency dependence of complex dielectric permittivity for the borehole and the formation are fixed. R corresponds to the receiver's position and T to that of the source of the harmonic magnetic field.

- The method of finding porosity and water saturation is accurate
- The equivalent semistationary circuit (Fig.8) works for this frequency range

Measuring the polarization parameters with the borehole inductive tool

Levitskaya performed lab measurements of dielectric spectra within the 50 Hz to 80 MHz frequency interval in a capacitor cell [Levitskaya, Sternberg, 1996] using the resonance method. To eliminate polarization next to the electrodes in the low-frequency domain on water-saturated samples, a 0.08 to 0.1 mm polyethylene film was glued to the sides of the samples; this film does not have dispersion in the

Table 4—The models of water-and-oil-saturated media. The first sample is water-saturated dolomite and the other samples are saturated sandstones. The dielectric spectra of corresponding samples are presented in Fig. 23 and 24.

Sample No.	Fluid in sample	Φ, %	Φ_{oil}, %	Φ_{water}, %
1	Fresh water	16.9	0	16.9
2	Oil	NA	NA	-
3	Water (brine)	14	0	14
4	Water-oil	14	7	7

frequency range of the measured electromagnetic field. Dielectric permittivity and the tangent of the loss angle for the film are: $\mathrm{Re}\varepsilon = 2.3$, $tg\delta = 0.0004$. The measurements of the tangent of the loss angle were performed using the resonance method with the Q-meter. The measurement system of the two-layer capacitor was represented with two serially connected capacitors. The measured tangent of the loss angle for the two-layer capacitor may be estimated using the following formula [Akhadov, 1977]:

$$tg\delta = \frac{\mathrm{Re}\varepsilon_2\theta_2 tg\delta_2 + \mathrm{Re}\varepsilon_1\theta_1 tg\delta_1}{\mathrm{Re}\varepsilon_2\theta_2 + \mathrm{Re}\varepsilon_1\theta_1},$$

where θ_2, θ_1 are the bulk fractions of the flat film and the sample. Because the film thickness and its tangent of the loss angle are small compared to the corresponding parameters of the sample, $tg\delta = tg\delta_1$. In other words, it was the tangent of the loss angle that was being measured, within the stated measurement error bars. On the other hand, because of extremely low conductivity of the polyethylene film, with respect to the direct current, the loss currents are small in the capacitor representing it, and the loss currents must be identified explicitly in the loss factor:

$$tg\delta = tg\delta + \frac{\mathrm{Im}\varepsilon_1 + \sigma_0/\varepsilon_0\omega}{\mathrm{Re}\varepsilon_1}.$$

σ_0 denotes conductivity of the sample with ε_0 respect to direct current with being the dielectric permittivity of vacuum. The latter fact was not pointed out by Levitskaya, even though the loss factor she measured included direct ohmic losses. In this case, the value σ_0 may be measured using the asymptotic value of $\sigma_0/\varepsilon_0\omega$ of the spectral dependence $\mathrm{Im}\varepsilon + \sigma/\varepsilon_0\omega$ in the low-frequency part of the spectrum. This is important if the borehole spectral inductive tools that also measure the value $\mathrm{Im}\varepsilon + \sigma/\varepsilon_0\omega$ are taken into consideration, because, in the harmonic representation, dependence of conductivity and the imaginary part of dielectric permittivity is reflected in the Maxwell equations as $\mathrm{Im}\varepsilon + \sigma/\varepsilon_0\omega$. Therefore, the question arises as to whether the electromagnetic inductive borehole tool can measure the dielectric polarization spectrum.

A study of the possibility of using inductive borehole logging to measure dielectric parameters of the formation saturated with a water-oil mixture requires solving the set of Maxwell equations for the borehole filled with mud and surrounded by the formation being studied.

The influence of dispersion of dielectric permittivity of water- and oil-saturated formation beyond the borehole upon the amplitude of the longitudinal component of the magnetic field at the axis of the OBM-filled borehole was studied. The dielectric characteristics of mud in the MHz range of the electromagnetic field are considered given [Patil et al. 2010] and are presented in **Fig. 20** and **21**. Instead of the imaginary part of dielectric permittivity, ε'' the value reciprocal to the loss factor is presented.

In the axisymmetric case, the electromagnetic field is obtained with the following components: $\mathbf{B} = (B_r, 0, B_z)$, $\mathbf{E} = (0, E_\varphi, 0)$, $\mathbf{H} = (H_r, 0, H_z)$, $\mathbf{D} = (0, D_\varphi, 0)$, $\mathbf{j} = (0, j_\varphi, 0)$. The Maxwell equations in the cylindrical system of coordinates are expressed via the Fourier presentation with respect to time for the domain "in" ($0 < r < r_b$) and domain "ext" ($r_b < r < \infty$) as:

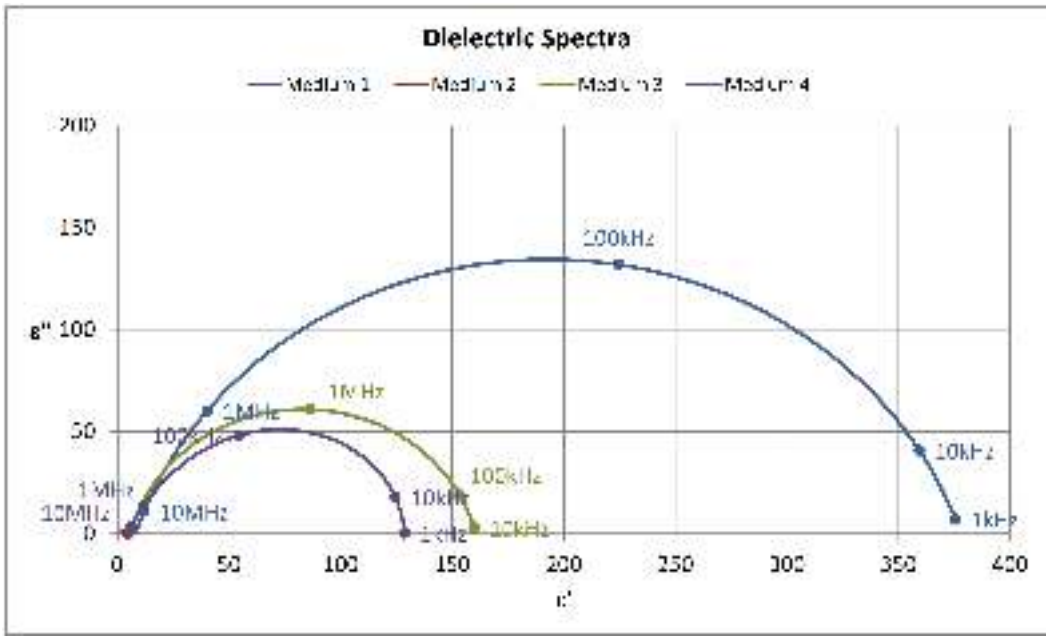

Figure 23—The dielectric spectra [Levitskaya, 1984] [Levitskaya, Palveleva; 1990] for the samples saturated with various fluids. The line with squares is the spectrum corresponding to the sample saturated with fresh water. The line with diamonds is the spectrum corresponding to the sample saturated with brine (15 g/L NaCl). The line with triangles is the spectrum corresponding to the sample saturated with the water-oil mixture (salinity of water being 15 g/L NaCl). Fig. 24 shows the spectrum corresponding to Medium 2.

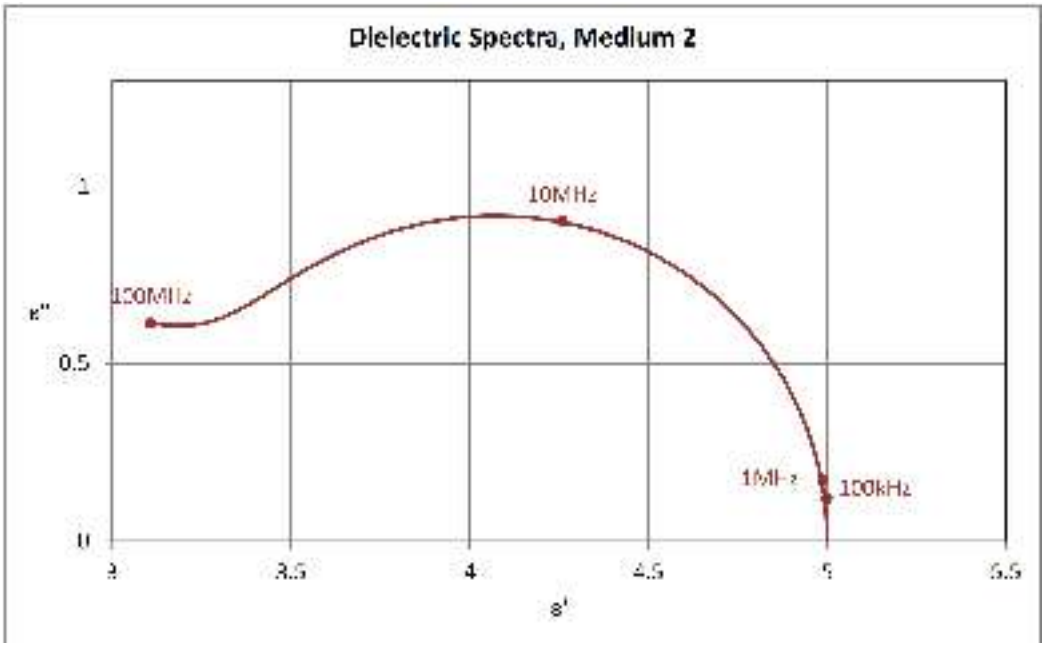

Figure 24—The dielectric spectrum of oil-saturated sandstone (Revizskij, Dyblenko; 2002), Medium 2.

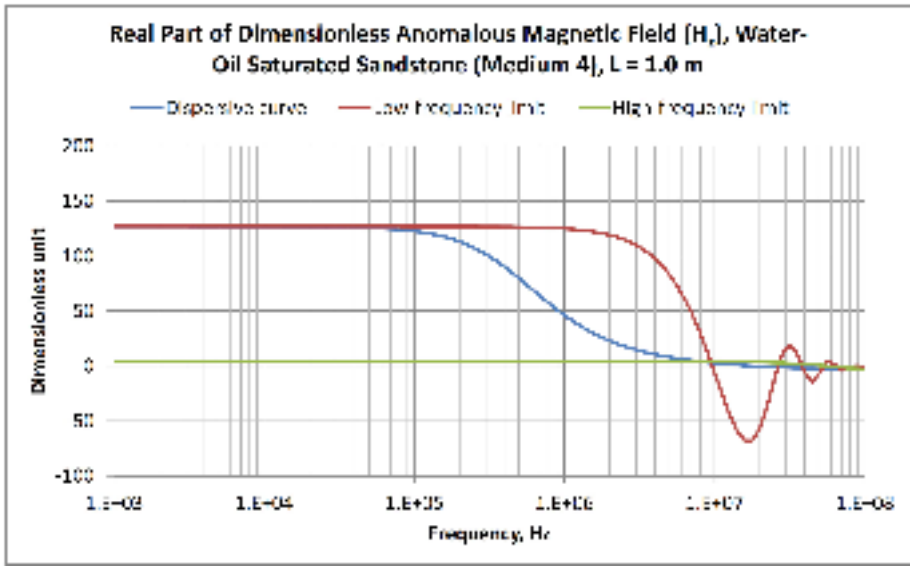

Figure 25—The real part of dielectric permittivity of the magnetic field at the borehole axis at a distance of 1.0 m from the radiation source. The dash-dotted line corresponds to the real part of dielectric permittivity in the low-frequency limit; the solid line corresponds to the real part of dielectric permittivity in the high-frequency limit. The dashed line corresponds to the frequency-dependent value of dielectric permittivity for sample 4 (see Fig. 23). The borehole radius is 10.8 cm and the borehole is filled with OBM (see Fig. 20, Fig. 21.)

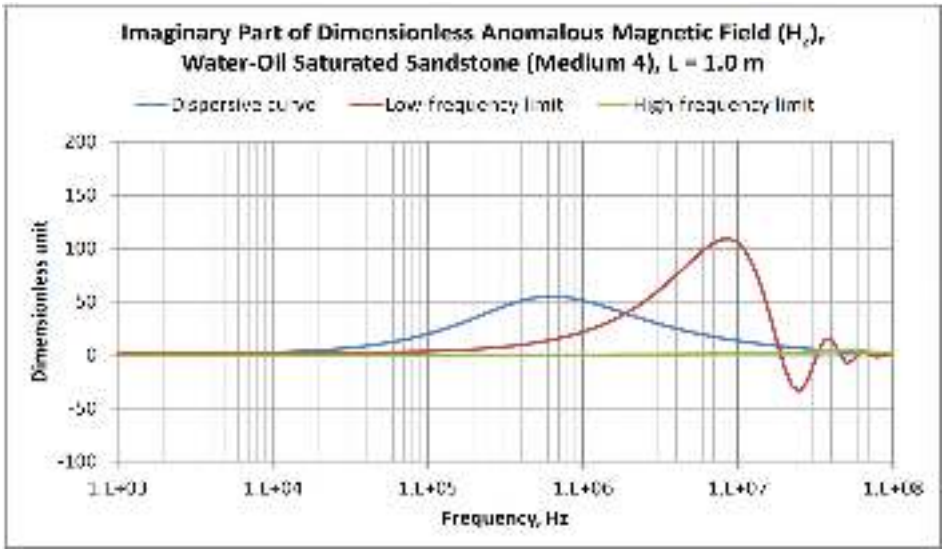

Figure 26—The imaginary part of dielectric permittivity of the magnetic field at the borehole axis at a distance of 1.0 m from the radiation source. The dash-dotted line corresponds to the imaginary part of dielectric permittivity in the low-frequency limit and the solid line corresponds to the imaginary part of dielectric permittivity in the high-frequency limit. The dashed line corresponds to the frequency-dependent value of dielectric permittivity for sample 4 (see Fig. 23). The borehole radius is 10.8 cm and the borehole is filled with OBM (see Fig. 20, Fig. 21).

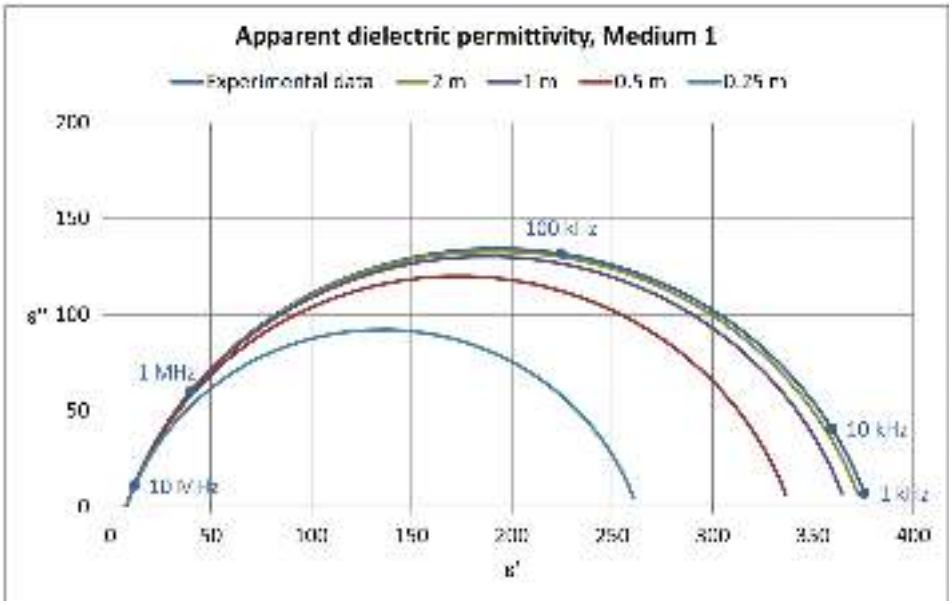

Figure 27—Apparent dielectric spectra in the medium with a borehole. The borehole radius is 10.8 cm and the borehole is filled with OBM whose dielectric spectrum is shown in Fig. 20 and 21. The medium beyond the borehole corresponds to sandstone saturated with water and oil in Medium 4 (see the polarization curve in Fig. 23).

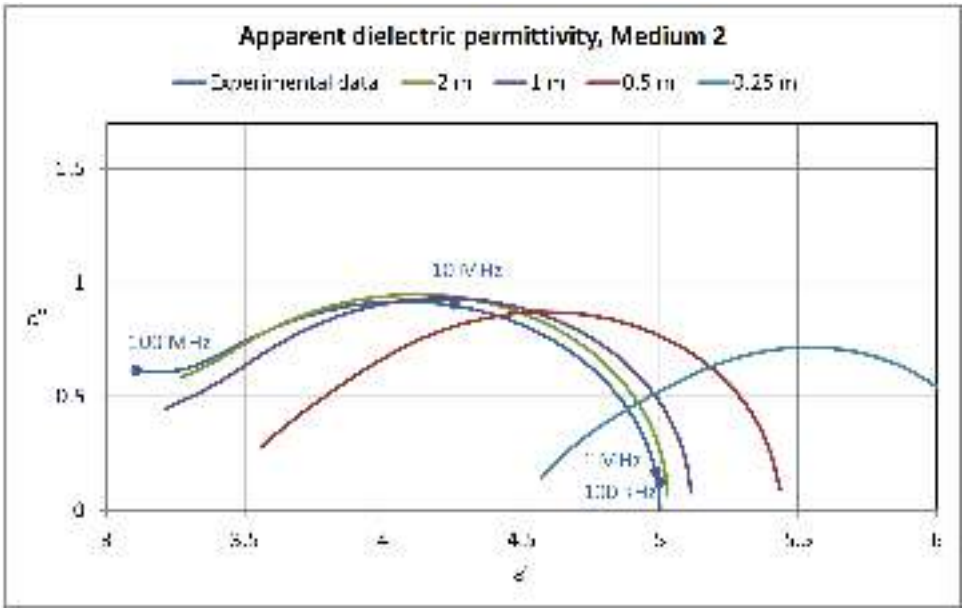

Figure 28—Apparent dielectric spectra in the medium with a borehole. The borehole radius is 10.8 cm and the borehole is filled with OBM whose dielectric spectrum is shown in Fig. 20 and 21. The medium beyond the borehole corresponds to sandstone saturated with oil, Medium 2 (see polarization curve in Fig. 24).

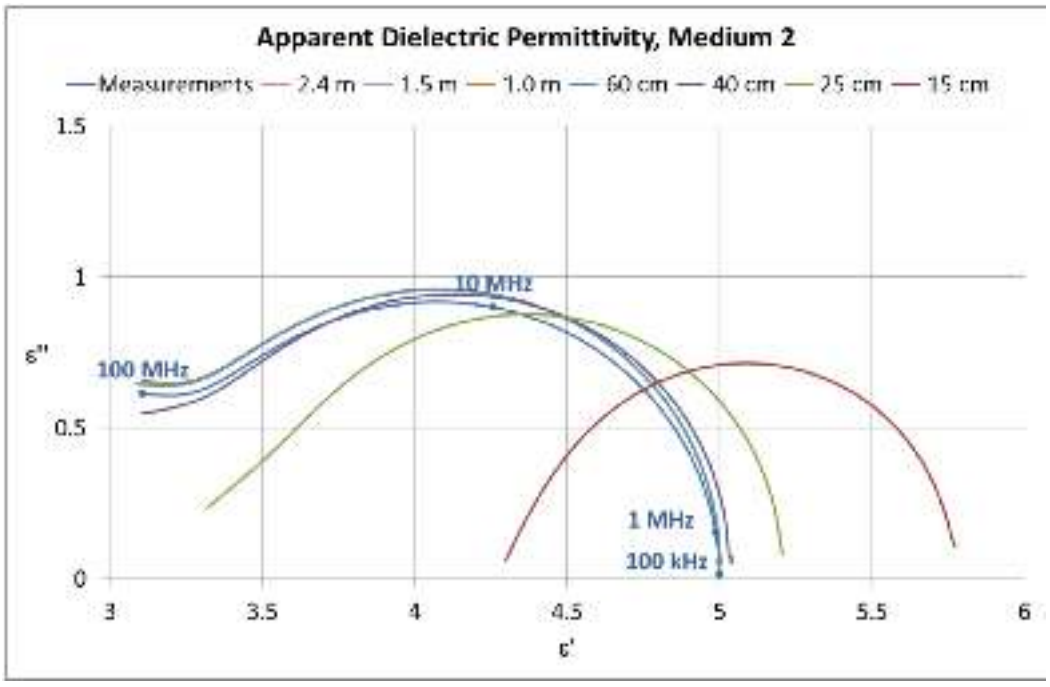

Figure 29—Apparent dielectric spectra of the three-coil probes in the medium with a borehole. The borehole radius is 10.8 cm and the borehole is filled with OBM whose dielectricc spectrum is shown in Fig. 20 and 21. The medium beyond the borehole corresponds to sandstone saturated with oil, Medium 2 (see the polarization curve in Fig. 24).

$$\left\{\begin{array}{l} \dfrac{\partial H_r^{in}}{\partial z} - \dfrac{\partial H_z^{in}}{\partial r} = (\sigma_{0,b} - i\omega\varepsilon_0\varepsilon_b)E_\varphi^{in} \\ \dfrac{1}{r}\dfrac{\partial E_z^{in}}{\partial \varphi} - \dfrac{\partial E_\varphi^{in}}{\partial z} = i\omega\mu_0 H_r^{in} \\ \dfrac{1}{r}\dfrac{\partial}{\partial r}(rE_\varphi^{in}) - \dfrac{1}{r}\dfrac{\partial E_r^{in}}{\partial \varphi} = i\omega\mu_0 H_z^{in} - i\omega\mu_0 M\,\delta(\mathbf{r}) \\ \dfrac{1}{r}\dfrac{\partial}{\partial r}(rH_\varphi^{in}) + \dfrac{\partial H_r^{in}}{\partial z} = 0 \end{array}\right. \quad \left\{\begin{array}{l} \dfrac{\partial H_r^{ext}}{\partial z} - \dfrac{\partial H_z^{ext}}{\partial r} = (\sigma_{0,f} - i\omega\varepsilon_0\varepsilon_f)E_\varphi^{ext} \\ \dfrac{1}{r}\dfrac{\partial E_z^{ext}}{\partial \varphi} - \dfrac{\partial E_\varphi^{ext}}{\partial z} = i\omega\mu_0 H_r^{ext} \\ \dfrac{1}{r}\dfrac{\partial}{\partial r}(rE_\varphi^{ext}) - \dfrac{1}{r}\dfrac{\partial E_r^{ext}}{\partial \varphi} = i\omega\mu_0 H_z^{ext} \\ \dfrac{1}{r}\dfrac{\partial}{\partial r}(rH_\varphi^{ext}) - \dfrac{\partial H_r^{ext}}{\partial z} = 0 \end{array}\right.$$

The last equation in the system "in" takes into account that a vertical magnetic dipole is present in the point $r = (0, 0, 0)$ as a point-like source. At the interface between the borehole and the porous formation $r = r_*$, the continuity conditions for the tangent and normal components hold true.

$$\left[\mathbf{E}^{in} - \mathbf{E}^{ext}\right]\cdot\boldsymbol{\tau} = 0, \quad \left[\mathbf{D}^{in} - \mathbf{D}^{ext}\right]\cdot\mathbf{n} = 0, \quad \left[\mathbf{H}^{in} - \mathbf{H}^{ext}\right]\cdot\boldsymbol{\tau} = 0, \quad \left[\mathbf{B}^{in} - \mathbf{B}^{ext}\right]\cdot\mathbf{n} = 0.$$

At infinity, outside the borehole, there is no electromagnetic field. Ohm's law $\mathbf{j} = \sigma_0\mathbf{E}$ introduces conductivity with respect to direct current σ_0. Assuming the medium is non-magnetic, a simple material equation $\mathbf{B}(\omega) = \mu_0\mathbf{H}(\omega)$, $\mu_0 = 4\pi\cdot 10^{-7}\ H\cdot m^{-1}$ is obtained. Next, introduce the frequency-dependent dielectric permittivity $\varepsilon(\omega)$ $\mathrm{Re}\,\varepsilon + i\,\mathrm{Im}\,\varepsilon$: $\mathbf{D}(\omega) = \varepsilon_0\varepsilon(\omega)\mathbf{E}(\omega)$, where c is the velocity of light in the vacuum. For the imaginary part of complex dielectric permittivity and the loss factor ε'', the following notations are used:

$$\varepsilon^* = \varepsilon + \frac{i\sigma_0}{\omega\varepsilon_0} = \varepsilon' + i\varepsilon'', \quad \varepsilon' = \mathrm{Re}\,\varepsilon^*, \quad \varepsilon'' = \mathrm{Im}\,\varepsilon^* = \frac{\sigma_0}{\omega\varepsilon_0}, \quad \sigma = \omega\varepsilon_0\varepsilon''.$$

In Maxwell's equations, $\sigma_{0,b}$, ε_b (ω) are conductivity with respect to direct current and frequency dependence of dielectric permittivity of mud; $\sigma_{0,f}$, ε_f (ω) are conductivity with respect to direct current and frequency dependence of dielectric permittivity of the formation beyond the borehole.

Table 5—The sizes of the three-coil probes.

Probe No.	Location of the first coil $L^{(1)}$, m	Location of the second coil $L^{(2)}$, m
1	0.12	0.15
2	0.19	0.25
3	0.30	0.40
4	0.46	0.60
5	0.70	1.0
6	1.08	1.5
7	1.67	2.4

The solution to the borehole equations (the "in" domain) is a summation of fields:

$$\mathbf{H}^{\cdot} = \mathbf{H}_0^{\cdot} + \mathbf{H}_1^{\cdot},\ \mathbf{E}^{\cdot} = \mathbf{E}_0^{\cdot} + \mathbf{E}_1^{\cdot},\ \mathbf{D}^{\cdot} = \mathbf{D}_0^{\cdot} + \mathbf{D}_1^{\cdot},\ \mathbf{B}^{\cdot} = \mathbf{B}_0^{\cdot} - \mathbf{B}_1^{\cdot},\ \mathbf{j}^{\cdot} = \mathbf{j}_0^{\cdot} - \mathbf{j}^{\cdot}, \text{ such that:} \tag{8}$$

$$\begin{gathered}
\frac{\partial \mathbf{H}_{0,r}^{\cdot}}{\partial z} - \frac{\partial \mathbf{H}_{0,z}^{\cdot}}{\partial r} = \left(\sigma_{1,0} - i\omega\varepsilon_0\varepsilon_1\right)\mathbf{E}_{1,\varphi}^{\cdot}, \quad \frac{1}{r}\frac{\partial}{\partial r}\left(r\mathbf{H}_{0,\varphi}^{\cdot}\right) + \frac{\partial \mathbf{H}_{0,z}^{\cdot}}{\partial z} = 0 \\
\frac{1}{r}\frac{\partial \mathbf{E}_{1,z}^{\cdot}}{\partial \varphi} - \frac{\partial \mathbf{E}_{1,\varphi}^{\cdot}}{\partial z} - i\omega\mu_0\mathbf{H}_{0,r}^{\cdot}, \quad \frac{1}{r}\frac{\partial}{\partial r}\left(r\mathbf{E}_{0,\varphi}^{\cdot}\right) - \frac{1}{r}\frac{\partial \mathbf{E}_{0,r}^{\cdot}}{\partial \varphi} - i\omega\mu_0\mathbf{H}_{0,z}^{\cdot} - i\omega\mu_0 M_z\sigma(x)\sigma(y)\dot{\sigma}(z), \text{ and} \\
\frac{\partial \mathbf{H}_{1,\varphi}^{\cdot}}{\partial z} - \frac{\partial \mathbf{H}_{1,z}^{\cdot}}{\partial r} = -\left(\sigma_{2,0} - i\omega\varepsilon_0\varepsilon_2\right)\mathbf{E}_{1,r}^{\cdot}, \quad \frac{1}{r}\frac{\partial}{\partial r}\left(r\mathbf{H}_{1,\varphi}^{\cdot}\right) + \frac{\partial \mathbf{H}_{1,r}^{\cdot}}{\partial z} = 0 \\
\frac{1}{r}\frac{\partial \mathbf{E}_{1,r}^{\cdot}}{\partial \varphi} - \frac{\partial \mathbf{E}_{1,\varphi}^{\cdot}}{\partial z} = i\omega\mu_0\mathbf{H}_{1,r}^{\cdot}, \quad \frac{1}{r}\frac{\partial}{\partial r}\left(r\mathbf{E}_{1,\varphi}^{\cdot}\right) - \frac{1}{r}\frac{\partial \mathbf{E}_{1,r}^{\cdot}}{\partial \varphi} = i\omega\mu_0\mathbf{H}_{1,z}^{\cdot}.
\end{gathered} \tag{9}$$

Outside the borehole (the "ext" domain), the field equations keep their form. The solution for the zero-field (8) (where the field amplitudes are denoted with a zero subscript) describing the homogeneous infinite medium filled with mud is known [A.A. Kaufman, 1965]

$$\begin{gathered}
\mathbf{E}_{0,\varphi}^{\cdot} = i\omega\mu_0\frac{M_z r}{4\pi R^3}\left(1 - ikR\right)e^{-ikR}, \ \mathbf{H}_{0,r}^{\cdot} = \frac{M_z rz}{4\pi R^5}\left(3 + 3ikR - k^2R^2\right)e^{-ikR}, \\
\mathbf{H}_{0,z}^{\cdot} = -\frac{M_z}{4\pi R^3}\left(3\frac{r^2}{R^2} + 3ik\frac{r^2}{R} + k^2R^2 - 2 - 2ikR\right)e^{-ikR}, \\
R^2 = r^2 + z^2, \ k^2 = -i\omega\mu_0\sigma_{0,0} - \omega^2\mu_0\varepsilon_0\varepsilon_0.
\end{gathered} \tag{10}$$

Knowing the amplitudes of the electric and magnetic field for the zero-field (10) enables the amplitudes of the electromagnetic field to be obtained with the subscript "1" in the borehole at the symmetry axis*(r=0)* from (9) and the corresponding boundary conditions:

$$\begin{gathered}
\mathbf{H}_{1,z}^{\cdot} = \frac{1}{\pi}\int_0^{\infty} D\cos(\zeta z)\,d\zeta, \ D = \frac{p_1K_0(p_1r_1)K_1(p_2r_2) - p_2K_0(p_2r_2)K_1(p_1r_1)}{p_1I_0(p_1r_1)K_1(p_2r_2) - p_2K_0(p_2r_2)I_1(p_1r_1)} \\
p_1 = \zeta^2 - k_1^2, \quad k_1^2 = -i\omega\mu_0\sigma_{0,1} - \omega^2\mu_0\varepsilon_0\varepsilon_1, \\
p_2 = \zeta^2 - k_2^2, \quad k_2^2 = -i\omega\mu_0\sigma_{0,2} - \omega^2\mu_0\varepsilon_0\varepsilon_2,
\end{gathered} \tag{11}$$

where $I_{0,1}$ are the infield functions and $K_{0,1}$ are the Macdonald functions.

To solve the forward problem of computing the fields at the symmetry axis, the dielectric spectra of four samples with various porosity and fluid content were selected (see **Table 4**).

For illustration purposes, the spectrum corresponding to the oil-saturated medium (Medium 2) is shown in Fig. 24, because its complex dielectric permittivity is much smaller than that of the other samples. Fig. 23 shows the spectrum of dielectric permittivity corresponding to the sample saturated with fresh water differs greatly from the spectrum of the sample saturated with the water-oil mixture (especially with respect to polarization). The sample saturated with fresh water (Medium 1) is represented by the Cole-Cole polarization. The sample saturated with the water-oil mixture is represented by the Havriliak-

Negami polarization. The spectra corresponding to the water-saturated samples (Medium 1, Medium 3) are symmetrical regardless of salinity, whereas the spectrum corresponding to the sample saturated with the water-oil mixture (Medium 3) is asymmetrical.

The anomalous magnetic field is obtained using the formula:

$$\mathbf{H}_z' = \mathbf{H}_z - \frac{M_z}{2\pi L^3}.$$

where L is the distance from the source (magnetic dipole) to the receiver. The dimensionless anomalous magnetic field is:

$$\mathbf{II}' = \frac{2\pi L^3}{M_z \omega^2} \mathbf{H}_z'.$$

Taking into account the possibility of measuring the magnetic field with the accuracy of 1.0%, the 10 kHz to 100 MHz range in the figure shows that the tool is capable of identifying the dispersion effects during borehole logging (Fig. 27). Knowing that it is the Cole-Cole polarization the angles of the intersection are restored between the polarization curve and the axis representing the real part of dielectric permittivity. These data are necessary for finding the water content in the water-saturated formation.

The concept of apparent dielectric spectrum is introduced when formation parameters are restored from measured magnetic fields H_z via formulae (10) for the homogeneous medium: the apparent dielectric spectrum ε^a is a frequency function with complex values which satisfies the equation:

$$H_z = \frac{M_z}{2\pi L^3}(1 + ikL)e^{-ikL}, \quad k^2 = -\omega^2 \mu_0 \varepsilon_0 \varepsilon^a. \tag{12}$$

H_z is the measured magnetic field at the axis in the "in" the system with a borehole.

The solid line in Fig. 28 indicates the dielectric spectrum of a sandstone sample measured in the lab (Medium 4, Table 1). Using formula (11), the real and imaginary parts of the magnetic field for the medium with this spectrum of dielectric permittivity are obtained as defined by the blue curve for various lengths L. The apparent dielectric spectra for L are calculated as per (12). The dot-dashed, long-dashed and short-dashed lines in Fig. 28 represent the restored spectra. There is good dielectric transmission ability of the borehole two-coil in the 1 kHz to 100 MHz frequency range for water-saturated formations (high values of the loss factor and dielectric permittivity) for fairly long probes.

However, in the MHz frequency range of the electromagnetic field, transmission ability of the borehole two-coil inductive tool is insufficient even for long probes when the formation is saturated with oil.

For a three-coil probe, attenuation ***Att*** and phase difference ***DPh*** of the electromagnetic signal can be calculated from the formula:

$$Att = 20\log\left(\frac{|H_z^{(1)}|}{|H_z^{(2)}|}\left(\frac{L^{(1)}}{L^{(2)}}\right)^3\right), \quad DPh = \frac{180^\circ}{\pi}\arg\left(\frac{H_z^{(1)}}{H_z^{(2)}}\right)$$

$L^{(1)}$ is the distance from the source to the closest receiver coil and $L^{(2)}$ is the distance from the source to the farthest receiver coil. The magnetic field in the closest coil is $H_z^{(1)}$ and the magnetic field in the farthest (away) coil is $H_z^{(2)}$.

The apparent dielectric spectrum ε^a for the three-coil probe is introduced when the values of complex dielectric permittivity of the formation are restored from measured attenuations and phase differences of the magnetic fields $H_z^{(1)}$ and $H_z^{(2)}$ using the formulae:

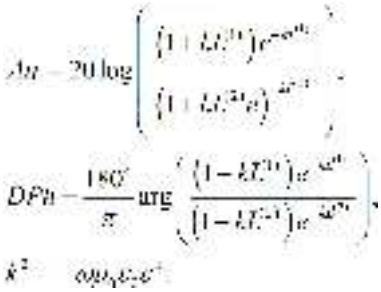

Fig. 29 shows the three-coil probes measure dielectric spectra accurately in the 1 kHz to 100 MHz frequency range of the electromagnetic field even when the base is 40 cm and larger.

Conclusions

Within the acoustic range of the electromagnetic field, and within borehole dielectric logging conditions, a quality criterion can be introduced to distinguish between water-saturated reservoirs and those saturated with a mixture of water and oil. The dielectric spectra of water-saturated reservoirs within the acoustic range of the electromagnetic field are characterized by the Cole-Cole polarization curve, whereas the dielectric spectra of water-and-oil-saturated reservoirs are characterized by the Havriliak-Negami polarization curve. Using the criterion and the main properties of Havriliak-Negami polarization parameters, two innovative methods of measuring porosity are proposed. An innovative method of measuring the water-oil ratio is proposed using known polarization dielectric parameters. The method proposed is an alternative to the one using mixing formulae and enables porosity and water-oil ratio to be attained for a porous formation saturated with a mixture of water and oil.

References

Akhadov Ya.Yu. *Dielectric Properties of Binary Solutions*. Moscow, USSR: Nauka, 1977 400 p.

Derevyanko A.I., Kurilenko O.D. Analysis of dielectric relaxation in the plane of complex dielectric permittivity // *Physical and Chemical Mechanics and Liophilicity of Dispersed Systems*. Kyev, USSR: Naukova Dumka, 1971, V.**2,** P.141–147.

Dukhin S.S., Shilov V.N. *Dielecgric Phenomena and Double Layer in Dispersed Systems and Poly-Electrolites*. Kyev, USSR: Naukova Dumka, 1972, 206 p.

Kaufman A.A. *Theory of Inductive Logging,* Novosibirsk, USSR: Nauka, 1965, 235 p.

Levitskaya Ts.M. Dielecgric relaxation in rocks // *Earth Physics (Proceedings of USSR Academy of Science),* 1984, V. **10,** P. 82–87.

Levitskaya Ts.M., Nosova E. N. Analysis of relaxation parameters of inter-surface polarization of rocks // *Earth Physics (Proceedings of USSR Academy of Science),* 1984, V. **10,** P. 88–93.

Levitskaya Ts.M., Palveleva I. I. Influence of hydrocarbons on sandstone dielectric spectrum // *Earth Physics (Proceedings of USSR Academy of Science),* 1990, V. **6,** P. 106–110.

Revizskij Yu.V., Dyblenko V.P. *A Study and Foundations of Physical Methods of Formation Oil Recovery Mechanism,* Moscow, Russia: Nedra Business Center ltd., 2002, 317 p.

Chelidze T. L., Derevyanko A.I., Kurilenko O.D. *Electric Spectroscopy of Heterogeneous Systems,* Kyev, USSR: Naukova Dumka, 1977, 232 p.

Bruggeman D.A.G. Berechnung verschiedener physikalischer Konstanten von heterogenen Substanzen // *Annalen der Physik,* vol. **416,** Issue 7, 1935, pp.636–664.

Hanai T. Kolloid. Z. 1961, **171,** 23.

Hizem M., Budan H., Deville B., Faiver O., Mosse L., Simon M. Dielectric Dispersion: A new wireline Petrophysical Measurement // *SPE 116130* (2008).

Levitskaya T.M., Sternberg B.K. Polorization processes in rocks 1. Complex Dielectric Permitivity method // *RadioScience,* Vol.**31,** N.4, 1996, pp.755–779.

Patil, P. A., Gorek, M., Folberth, M., Hartmann, A., Forgang, S., Fulda, C., et al. Experimental study of electrical properties of oil-based mud in the frequency range from 1 to 100 MHz // *SPE Drilling & Complition,* (2010, September), pp. 380–390.

Seleznev N., Boyd A., Habashy T., Luthi S.M. Dielectric mixing laws for fully and partially saturated carbonate rocks // SPWLA 45th Annual Logging Symposium, June 6-9, 2004.

Sen., P. and Feng, S. Geometrical model of conductive and dielectric properties of partially saturated rocks // *J.Appl.Phys.,* 1985, vol.**58**(8), pp. 3236–3243.